

# Mutations at the M2 and M3 Transmembrane Helices of the GABA<sub>A</sub>Rs $\alpha_1$ and $\beta_2$ Subunits Affect Primarily Late Gating Transitions Including Opening/Closing and Desensitization

Katarzyna Terejko,<sup>\*,§</sup> Michał A. Michałowski,<sup>§</sup> Ilona Izykowska, Anna Dominik, Aleksandra Brzóstowicz, and Jerzy W. Mozrzymas<sup>\*</sup>

Cite This: *ACS Chem. Neurosci.* 2021, 12, 2421–2436

Read Online

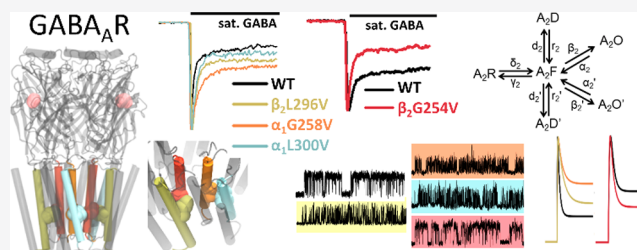
ACCESS |

Metrics & More

Article Recommendations

**ABSTRACT:** GABA type A receptors (GABA<sub>A</sub>Rs) belong to the pentameric ligand-gated ion channel (pLGIC) family and play a crucial role in mediating inhibition in the adult mammalian brain. Recently, a major progress in determining the static structure of GABA<sub>A</sub>Rs was achieved, although precise molecular scenarios underlying conformational transitions remain unclear. The ligand binding sites (LBSs) are located at the extracellular domain (ECD), very distant from the receptor gate at the channel pore. GABA<sub>A</sub>R gating is complex, comprising three major categories of transitions: openings/closings, preactivation, and desensitization. Interestingly, mutations at, e.g., the ligand binding site affect not only binding but often also more than one gating category, suggesting that structural determinants for distinct conformational transitions are shared. Gielen and co-workers (2015) proposed that the GABA<sub>A</sub>R desensitization gate is located at the second and third transmembrane segment. However, studies of our and others' groups indicated that other parts of the GABA<sub>A</sub>R macromolecule might be involved in this process. In the present study, we asked how selected point mutations ( $\beta_2$ G254V,  $\alpha_1$ G258V,  $\alpha_1$ L300V, and  $\beta_2$ L296V) at the M2 and M3 transmembrane segments affect gating transitions of the  $\alpha_1\beta_2\gamma_2$  GABA<sub>A</sub>R. Using high resolution macroscopic and single-channel recordings and analysis, we report that these substitutions, besides affecting desensitization, also profoundly altered openings/closings, having some minor effect on preactivation and agonist binding. Thus, the M2 and M3 segments primarily control late gating transitions of the receptor (desensitization, opening/closing), providing a further support for the concept of diffuse gating mechanisms for conformational transitions of GABA<sub>A</sub>R.

**KEYWORDS:** Desensitization, GABA<sub>A</sub> receptor, gating, transmembrane domain, opening/closing transitions, patch clamp



## INTRODUCTION

GABA type A receptors (GABA<sub>A</sub>Rs) belong to the pentameric ligand-gated ion channel (pLGICs) family, together with, e.g., ionotropic serotonin receptor type 3, glycine receptor, or nicotinic acetylcholine receptor. GABA<sub>A</sub>Rs play a crucial role in inhibitory synaptic transmission in the adult mammalian brain.<sup>1–3</sup> Dysfunction of GABAergic inhibition has been implicated in a number of neurological and psychiatric disorders such as epilepsy, autism, depression, and schizophrenia.<sup>4–8</sup> Moreover, GABA<sub>A</sub>Rs are targets of numerous endogenous and exogenous modulators including, for instance, neurosteroids, benzodiazepines, anesthetics, and barbiturates.<sup>9–13</sup> Recently, a major progress in determining the static structure of GABA<sub>A</sub>Rs has been achieved,<sup>14–17</sup> although the precise molecular scenarios underlying various conformational transitions of this receptors remain unclear. A characteristic feature of pLGICs is that the activation process comprises vast portions of the macromolecules as the ligand binding site (LBS), located at extracellular domain (ECD), is positioned

very far (approximately 50 Å)<sup>2,18</sup> from the receptor gate, suggesting complexity of gating mechanisms (Figure 1A–C). Another dimension of GABA<sub>A</sub>R gating complexity is numerous conformational transitions which can be grouped in three main categories, openings/closings, preactivation, and desensitization, and each of them may be represented by transitions into more than one state (especially for openings/closings and desensitization, typically more than one state are identified).<sup>19–23</sup>

It is known that there are two possible constriction points/gates in the pore, one at the 9' residue level, in the middle of the transmembrane domain (TMD), and the second one at the

Received: March 16, 2021

Accepted: May 25, 2021

Published: June 8, 2021



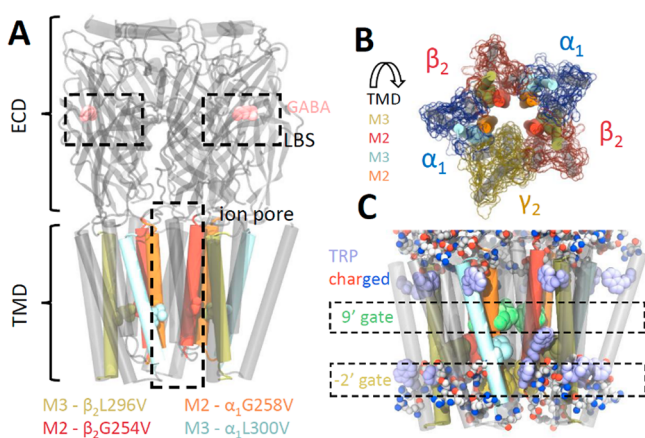


**Figure 1.** GABA<sub>A</sub>R structure and location of the  $\beta_2$ G254V,  $\alpha_1$ G258V,  $\alpha_1$ L300V, and  $\beta_2$ L296V residues. (A) General structure of GABA<sub>A</sub>R with marked ECD and TMD domains, LBSs and ion pore. Helices with investigated residues are marked in part A, with other helices in gray; subunit surfaces are marked in respective colors. Notice the long distance between these residues and LBSs. (B) TMD seen from the ECD vestibule. Helices with investigated residues are marked in part A, with other helices in gray; subunit surfaces are marked in respective colors. Notice the position of  $\alpha$ -helices (M2s lining the pore, M3s in the “inner ring” of helices bundles). (C) Close look at TMD with marked two constriction regions: 9' ( $\beta_2$ Leu259,  $\alpha_1$ Leu264, and  $\gamma_2$ Leu274, residues as green spheres) and -2' ( $\beta_2$ Ala248,  $\alpha_1$ Pro253, and  $\gamma_2$ Pro263, residues as yellow spheres) gates. Related to anchoring in the lipid membrane, tryptophan residues are marked as violet spheres. All charged residues are presented in spherical representation with atoms colored according to charge (red = negative, blue = positive, gray = neutral).

bottom, at the -2' residue level (Figure 1C). According to structural data, the first one is responsible for channel opening/closing, whereas the second one is related to desensitization. Interestingly, mutations at the LBS are commonly found to affect not only binding but also gating, typically altering not just one gating category but two or three of them.<sup>22,24–26</sup> This observation strongly suggests that structural determinants of the above-mentioned distinct gating transitions are not compartmentalized, but rather, specific structural elements of receptors might be shared upon different conformational transitions.

A particularly puzzling aspect with this respect is the process of desensitization. Gielen and co-workers<sup>27</sup> proposed that the functioning of the GABA<sub>A</sub>R desensitization gate is regulated by interactions between the second and third transmembrane segments which are in close vicinity of the abovementioned -2' residue, a presumed desensitization constriction site. However, studies from our group and others indicated involvement of other structural determinants in regulating the process of desensitization. We reported that a benzodiazepine, flurazepam, affected desensitization,<sup>24,28</sup> and when we consider that the binding site for this modulator is located at ECD, very distantly from transmembrane segments indicated by Gielen et al.,<sup>27</sup> it seems that desensitization might be also controlled by structures within ECD. Moreover, in our recent study,<sup>22</sup> we provided evidence that mutation of the F45 residue, located close to the agonist binding site at the loop G of the  $\alpha_1$  subunit, profoundly altered desensitization kinetics. Unexpectedly, we also found that mutation of the  $\alpha_1$ F14 and  $\beta_2$ F31 residues, located “above” the orthosteric binding site in ECD, also had a strong impact on the desensitization

transitions.<sup>21</sup> Thus, our studies suggest that desensitization might structurally depend on vast fragments of the GABA<sub>A</sub>R macromolecule, raising a concept of a “diffuse” desensitization gating mechanism rather than its well defined localization. This means that, although the site of the final step of the desensitization transition is located at the constriction of the ion pore (at the level of -2' residue in the TMD), the preceding structural rearrangements leading to this conformational change would comprise the vast parts of the macromolecule. Additionally, Germann and co-workers<sup>29</sup> observed that propofol shifted the active-desensitized equilibrium toward the active states and attributed this finding to altered agonist affinities at these conformations, thus emphasizing the importance of long-range cross talk between GABA binding site, modulator binding site, and gates for opening and desensitization. To further address the issue of the structural determinants of desensitization transitions in GABA<sub>A</sub>R, we asked to what extent selected point mutations ( $\beta_2$ G254V,  $\alpha_1$ G258V,  $\alpha_1$ L300V and  $\beta_2$ L296V, Figure 1A–C) at the presumed desensitization gate proposed by Gielen et al.<sup>27</sup> are specific for desensitization and to what extent they might also affect other conformational transitions of this receptor. Using high resolution macroscopic and single-channel recordings and analysis, we report that these substitutions, besides affecting desensitization, also profoundly altered openings/closings, having either no effect on preactivation or affecting it relatively weakly. Thus, the structure comprising the substituted residues appears to affect late gating transitions of the receptor, providing a further support for the concept of the diffuse gating mechanisms.

## RESULTS AND DISCUSSION

**Analysis of Macroscopic Currents Mediated by the  $\beta_2$ G254V,  $\alpha_1$ G258V,  $\beta_2$ L296V, and  $\alpha_1$ L300V Mutants Indicate Diversified Effects on the Receptor Gating.** We started to investigate the impact of the considered mutations at the bottom TMD area (M2 and M3 segments) on the receptor functions from assessment of agonist potency by analyzing the dose–response relationships (Figure 2). There was a slight reduction of EC<sub>50</sub> value for the  $\beta_2$ G254V mutant with respect to the WT receptor (31.6 vs 40.2  $\mu$ M); however, this change is deemed insignificant, as the respective dose–response relationships nearly overlapped. For other mutants, EC<sub>50</sub> value increased in ascending order for  $\alpha_1$ L300V,  $\beta_2$ L296V and  $\alpha_1$ G258V (Figure 2, inset). The largest change was for the

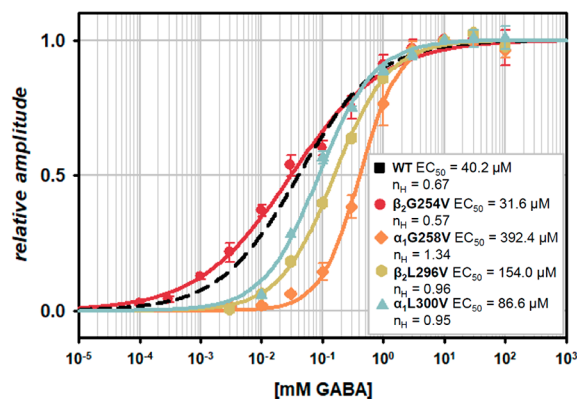


**Figure 2.** Mutations cause minor effects on agonist potency relative to WT.

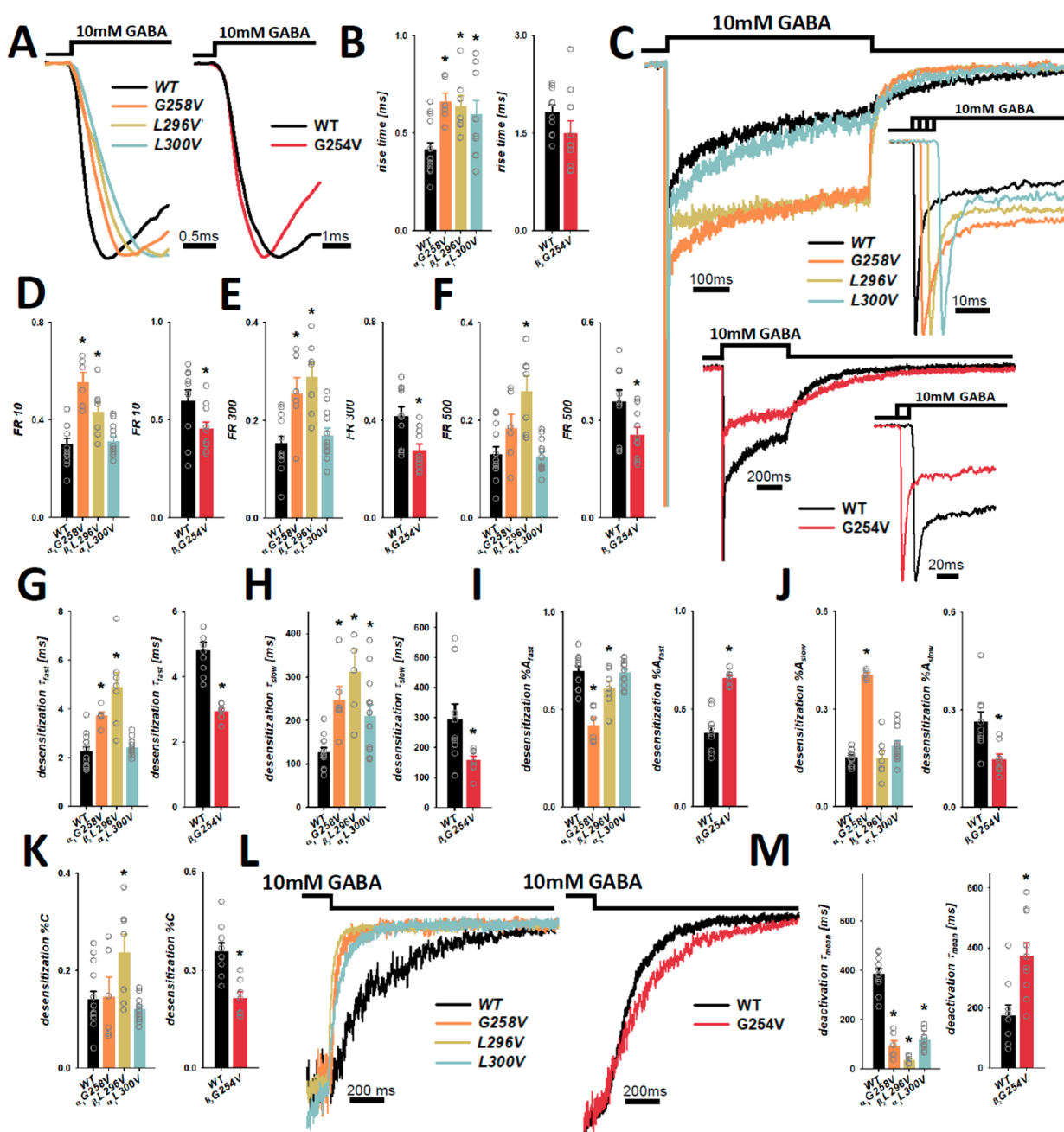


**Figure 3.** Kinetics of macroscopic currents evoked by saturating [GABA] applications is altered by the  $\beta_2$ G254V,  $\alpha_1$ G258V,  $\alpha_1$ L300V and  $\beta_2$ L296V mutations. (A) Typical normalized current traces of the onset phase, recorded from excised-patches, showing changes induced by the mutations in comparison to the WT receptors. Recordings presented for  $\beta_2$ G254V with respective control (right panel) were obtained in the whole-cell configuration (lifted-cell). (B) Statistics for rise time values. (C) Typical normalized current traces evoked by 500 ms saturating GABA application or the initial 80–100 ms (right panel), showing differences in the time course and extent of fast and slow components of macroscopic desensitization for the  $\alpha_1$ G258V,  $\alpha_1$ L300V,  $\beta_2$ L296V and  $\beta_2$ G254V mutants compared to the WT receptors. (D–F) Statistics for FR10, F300, and FR500 values. (G, H) Statistics for time constants of fast ( $\tau_{fast}$ ) and slow ( $\tau_{slow}$ ) macroscopic desensitization components. (I, J) Statistics for percentages of the aforementioned desensitization components. (K) Statistics for the percentage (%C) of the stationary nondesensitizing current phase. (L) Typical normalized current traces representing effects of the  $\alpha_1$ G258V,  $\alpha_1$ L300V and  $\beta_2$ L296V mutations (left traces) and the  $\beta_2$ G254V mutant (right traces) on deactivation kinetics. (M) Statistics for mean deactivation time constant ( $\tau_{mean}$ ). The insets above the current traces represent agonist application. Statistically significant differences between the mutants and WT are marked with asterisks. For absolute values see Table 1.

$\alpha_1$ G258V mutant (392.4  $\mu$ M) which was also accompanied by the largest alteration in the Hill coefficient (1.34 vs 0.63). Thus, in the case of agonist potency, relatively minor changes were observed, and the saturating GABA concentration for all of the mutants (and WT) was set at 10 mM. These trends in dose–response relationships suggest that the considered

mutations might have a relatively minor impact on the agonist binding step.

Dose–response relationships normalized to current amplitudes elicited by saturating GABA concentrations (10 mM for all of the mutants and the WT receptors) that were fitted with the Hill equation (eq 1, Materials and Methods). Black dashed

Table 1. Absolute Values Calculated for Kinetic Parameters in Macroscopic Current Analysis<sup>a</sup>

kinetic parameter	WT (EXP) <i>n</i> = 14	$\alpha_1$ G258V <i>n</i> = 6	$\beta_2$ L296V <i>n</i> = 7	$\alpha_1$ L300V <i>n</i> = 12	WT (LC) <i>n</i> = 10	$\beta_2$ G254V <i>n</i> = 10
rise time [ms]	0.41 ± 0.04	<b>0.66 ± 0.04*</b> <i>p</i> < 0.001	<b>0.64 ± 0.06*</b> <i>p</i> = 0.003	<b>0.60 ± 0.07*</b> <i>p</i> = 0.037	1.83 ± 0.19	1.50 ± 0.11
FR 10	0.30 ± 0.02	<b>0.56 ± 0.04*</b> <i>p</i> < 0.001	<b>0.43 ± 0.04*</b> <i>p</i> = 0.005	0.31 ± 0.02	0.60 ± 0.06	<b>0.45 ± 0.04*</b> <i>p</i> = 0.047
FR 300	0.15 ± 0.02	<b>0.26 ± 0.03*</b> <i>p</i> = 0.005	<b>0.29 ± 0.03*</b> <i>p</i> < 0.001	0.17 ± 0.01	0.42 ± 0.04	<b>0.28 ± 0.03*</b> <i>p</i> < 0.001
FR 500	0.13 ± 0.06	0.18 ± 0.03	<b>0.26 ± 0.03*</b> <i>p</i> < 0.001	0.13 ± 0.01	0.36 ± 0.04	<b>0.26 ± 0.02*</b> <i>p</i> = 0.030
$\tau_{fast}$ [ms]	2.27 ± 0.19	<b>3.71 ± 0.18*</b> <i>p</i> < 0.001	<b>4.90 ± 0.61*</b> <i>p</i> < 0.001	2.42 ± 0.10	4.82 ± 0.26	<b>2.94 ± 0.10*</b> <i>p</i> = 0.001
$\tau_{slow}$ [ms]	127.98 ± 9.92	<b>247.19 ± 31.88*</b> <i>p</i> < 0.001	<b>313.09 ± 51.82*</b> <i>p</i> = 0.001	<b>210 ± 26.47*</b> <i>p</i> = 0.021	294.69 ± 51.77	<b>158.48 ± 14.34*</b> <i>p</i> = 0.018
% $A_{fast}$	0.70 ± 0.02	<b>0.42 ± 0.04*</b> <i>p</i> < 0.001	<b>0.61 ± 0.04*</b> <i>p</i> = 0.042	0.69 ± 0.02	0.38 ± 0.10	<b>0.64 ± 0.07*</b> <i>p</i> = 0.007
% $A_{slow}$	0.15 ± 0.03	<b>0.41 ± 0.01*</b> <i>p</i> < 0.001	0.15 ± 0.02	<b>0.19 ± 0.02*</b> <i>p</i> = 0.041	0.26 ± 0.03	<b>0.15 ± 0.02*</b> <i>p</i> = 0.007
%C	0.14 ± 0.02	0.15 ± 0.04	<b>0.24 ± 0.04*</b> <i>p</i> = 0.013	0.12 ± 0.01	0.36 ± 0.03	<b>0.22 ± 0.02*</b> <i>p</i> < 0.001
deactivation $\tau_{mean}$ [ms]	383.87 ± 89.49	<b>93.40 ± 21.36*</b> <i>p</i> < 0.001	<b>36.03 ± 5.91*</b> <i>p</i> < 0.001	<b>116.50 ± 10.60*</b> <i>p</i> < 0.001	173.36 ± 37.31	<b>375.42 ± 43.17*</b> <i>p</i> = 0.003

<sup>a</sup>Significant changes relative to the respective WT control (EXP = excised-patch or LC = lifted-cell mode) are marked in bold with an asterisk (\*), and the corresponding *p* value is disclosed; *n* = number of patches.

line represents fitting with the Hill equation (eq 1) of the dose–response relationship obtained by Brodzki et al.<sup>30</sup> in the same experimental conditions. In the inset, EC<sub>50</sub> values and Hill coefficients (*n*<sub>H</sub>) for the respective mutants and the WT receptors as the control are presented.

Next, to check for the impact of the considered mutations on receptor gating, current responses elicited by saturating [GABA] (10 mM) were examined. As already mentioned in the Materials and Methods, for WT and all of the mutants except for  $\beta_2$ G254V, current traces were recorded from excised-patches, assuring the highest time resolution (Figure 3). For  $\beta_2$ G254V, recordings were carried out in the whole-cell configuration (lifted-cell mode) due to poor expression and were compared to recordings of currents mediated by the WT receptors in the same configuration (Figure 3). For each current trace, the following parameters were determined, rise time (RT); desensitization = FR10, FR300, FR500,  $\tau_{fast}$ , % $A_{fast}$ ,  $\tau_{slow}$ , % $A_{slow}$ , %C and deactivation =  $\tau_{mean}$  (eqs 2 and 3, Materials and Methods), and the absolute values for all these parameters are presented in Table 1. The mean rise time of current responses was significantly slower in the case of the  $\alpha_1$ G258V,  $\alpha_1$ L300V and  $\beta_2$ L296V receptors compared to WT (Figure 3A,B; Table 1). There was a slight trend to accelerate the current onset in the  $\beta_2$ G254V mutant; however, it was not significant, and importantly, recordings for this receptor were made in the lifted-cell mode in which solution exchange is markedly slower than in the case of excised-patches (compare RT for WT: 0.41 and 1.83 ms in excised-patch and lifted-cell, respectively; Figure 3A,B; Table 1).

Because the mutations are located at the presumed desensitization gate,<sup>27</sup> a particular care was taken in our analysis to characterize the macroscopic desensitization (hence numerous parameters describing this process in Table 1). The fraction of nondesensitized current was measured at 10, 300 and 500 ms after the peak (FR10, FR300 and FR500). For the  $\alpha_1$ G258V and  $\beta_2$ L296V mutants, FR10 and FR300 were significantly increased (for  $\beta_2$ L296V also FR500) with respect

to WT, indicating the decreased extent of desensitization (Figure 3C,E–G). Moreover, in these two mutated receptors, both fast and slow desensitization time constants,  $\tau_{fast}$  and  $\tau_{slow}$ , were slowed down, while percentages of the fast components, % $A_{fast}$ , were reduced compared to those of WT (% $A_{slow}$  increased only in  $\alpha_1$ G258V, Figure 3C,G–J; Table 1). Additionally, the stationary fraction of current (%C) was significantly increased for the  $\beta_2$ L296V mutant (Figure 3K; Table 1). Thus, the  $\alpha_1$ G258V and  $\beta_2$ L296V mutations slowed down the time course and reduced the extent of macroscopic desensitization (at least at some time points). In the case of the  $\alpha_1$ L300V mutation, we observed an increased value of the slow desensitization time constant,  $\tau_{slow}$ , with a minor (although significant) increase in percentage (% $A_{slow}$ ) of this component (Figure 3C,G–J; Table 1). We also analyzed desensitization characteristics for the  $\beta_2$ G254V mutant for which, as already mentioned, recordings were made in the lifted-cell mode. Contrary to the previously analyzed mutants, for the  $\beta_2$ G254V receptors, both the rate and extent of macroscopic desensitization were upregulated, although this effect was relatively small. Indeed, FR10, FR300 and FR500 were reduced, and fast and slow time constants  $\tau_{fast}$  and  $\tau_{slow}$  were accelerated (with % $A_{fast}$  increased and % $A_{slow}$  reduced); the stationary fraction of current (%C) was significantly reduced (Figure 3C–K; Table 1). We additionally analyzed the time course of deactivation (assessed as  $\tau_{mean}$ , see Materials and Methods) which was significantly accelerated for the  $\alpha_1$ G258V,  $\beta_2$ L296V and  $\beta_2$ L300V receptors, but for the mutation enhancing desensitization,  $\beta_2$ G254V, deactivation was slowed down with respect to WT (Figure 3L,M; Table 1).

**Kinetic Modeling of Macroscopic Data.** In order to provide detailed information regarding the impact of the considered mutations on receptor gating, model simulations were carried out using the optimization routine of ChannelLab software (see Materials and Methods). As pointed out by Colquhoun and Lape,<sup>31</sup> in general, macroscopic modeling is known to be susceptible to model overparametrization which

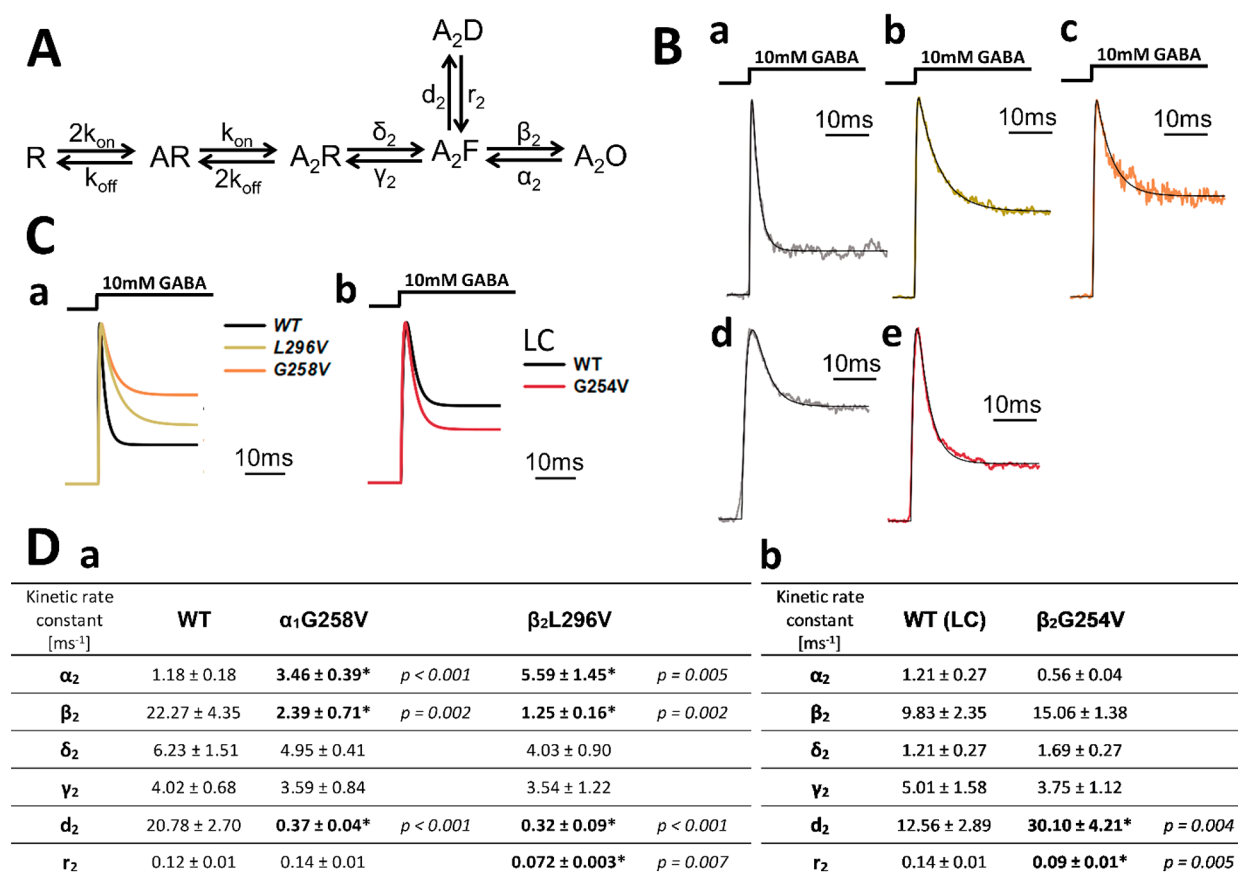


**Figure 4.** Macroscopic modeling indicates that  $\beta_2$ L296V and  $\alpha_1$ G258V affect the receptor gating differently than the  $\beta_2$ G254V mutation does. (A) Scheme of a kinetic model (fJWM from Szczot et al.<sup>26</sup>). In the scheme: R = unbound receptor; AR = singly bound receptor;  $A_2$ R = doubly bound receptor;  $A_2$ F = flipped state;  $A_2$ O = open state;  $A_2$ D = desensitized state. For all of the mutants, this model was used. (B) Exemplary model fits for recordings carried out in the excised-patch configuration for (a) WT receptors, (b)  $\beta_2$ L296V, (c)  $\alpha_1$ G258V, (d) WT in the lifted-cell mode, and (e)  $\beta_2$ G254V in the same mode. To improve the visibility, current traces for the WT receptors are drawn with a light gray line instead of a black one, as in part Ca,b. (C) (a, b) Normalized simulated traces for WT and the mutants generated for the mean values of the rate constants presented in parts Da and De, respectively, in the ~30 ms time window. Traces shown in part b were modeled for recordings from the lifted cells. (D) (a, b) Results of modeling presented in the table as mean values of the kinetic rate constants for each gating transition. Significant changes in the rate constants vs WT are marked in bold with an asterisk (\*), and the corresponding  $p$  value is disclosed. In part b, presented rates are for the lifted-cell mode recordings.

means that, in practice, it is hard to obtain stable and reproducible fits for complex models. For this reason, we carried out the macroscopic modeling for simplified schemes (simpler than in the case of single-channel data, see below).

In the case of the  $\alpha_1$ G258V and  $\beta_2$ L296V mutations, the major manifestations of the altered kinetic phenotype with respect to the WT receptors (slower onset and reduced rate and extent of rapid desensitization) could be observed within the time window of approximately 30 ms. We thus restricted our analysis for this time window and fitted the respective traces (for WT and the mutants) with a simplified model with one open and one (rapid) desensitized state (Figure 4A, exemplary fits in part Ba–c, simulated traces in part Ca). Using this approach, the values of the rate constants for the WT receptors (Figure 4Da) were comparable to those obtained in our previous studies<sup>24,26</sup> and the kinetic features of current responses mediated by these receptors were well-reproduced by curves obtained from modeling within the considered time range (data not shown). Also, in the case of the considered mutants, fitting with the simplified model to approximately 30 ms intervals of current responses well-reproduced the time course of recorded currents. As expected from observations on

macroscopic desensitization (Table 1), for both  $\alpha_1$ G258V and  $\beta_2$ L296V mutations, model fitting revealed a large and significant reduction of the desensitization rate  $d_2$ , and the resensitization  $r_2$  parameter was significantly decreased for  $\beta_2$ L296V but was unaltered for the  $\alpha_1$ G258V mutant (Figure 4Da). However, besides changes in the macroscopic desensitization ( $d_2$  and  $r_2$ ), these mutations also strongly affected the opening/closing transitions by dramatically reducing the opening  $\beta_2$  and by increasing the closing  $\alpha_2$  rates (Figure 4Da). The parameters that characterize preactivation ( $\delta_2$  and  $\gamma_2$ ) tended to be reduced in the case of both mutants, but these changes were not statistically significant. In Figure 4Ca, we show normalized simulated traces for WT and the mutants generated for the mean values of the rate constants presented in Figure 4Da, for the 30 ms time window. Taken altogether, the  $\alpha_1$ G258V and  $\beta_2$ L296V mutations showed a clear trend to impair late gating transitions (opening/closing and desensitization), having little or no effect on binding and preactivation.

The kinetic phenotype of currents mediated by the  $\beta_2$ L300V mutant was qualitatively different from that described above for  $\alpha_1$ G258V and  $\beta_2$ L296V. All the kinetic features related to desensitization were not different from those determined for

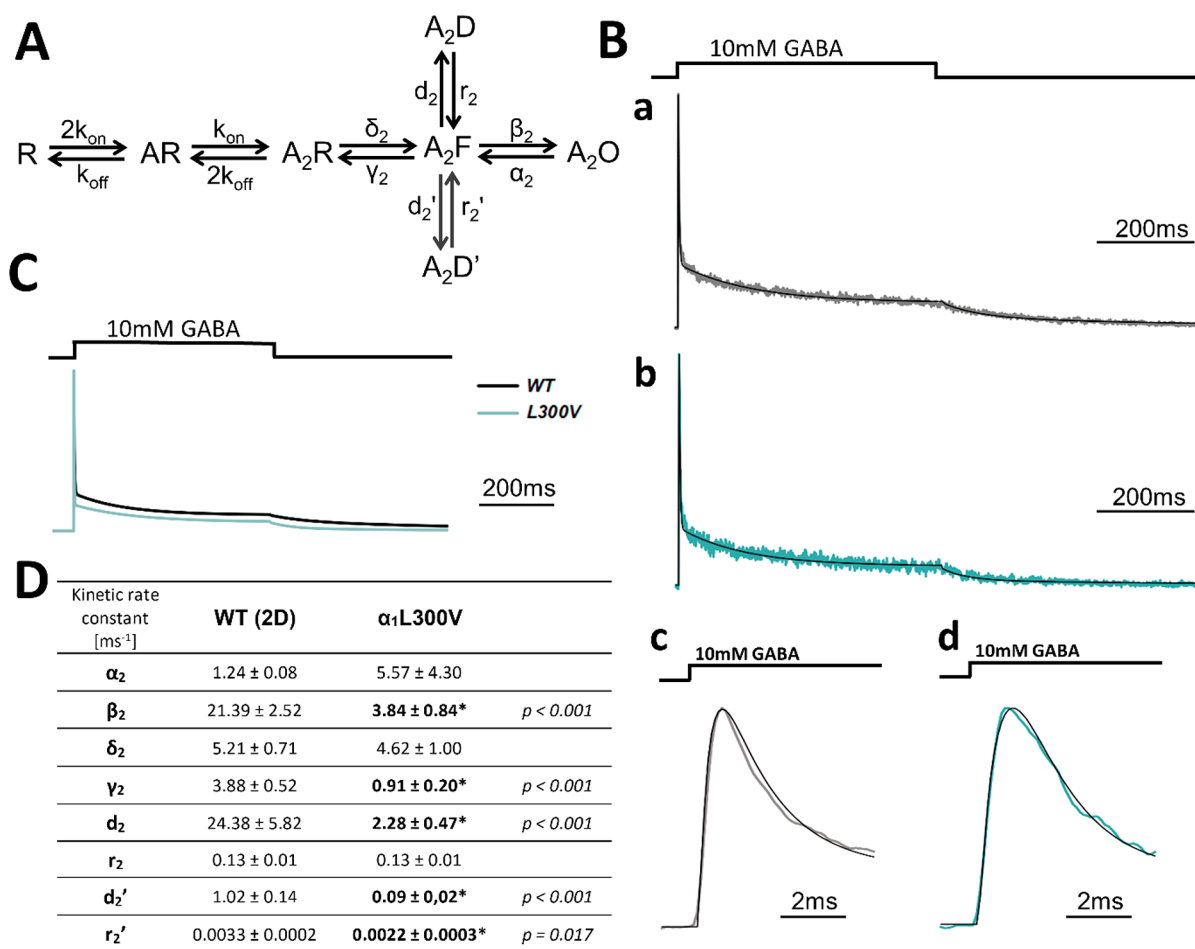


**Figure 5.** Macroscopic modeling indicates that the  $\alpha_1$ L300V mutation primarily affects the desensitization and opening rates. (A) Scheme of a kinetic model (fJWM from Szczot et al.<sup>26</sup>) with additional desensitized state. In the scheme: R = unbound receptor; AR = singly bound receptor;  $A_2R$  = doubly bound receptor;  $A_2F$  = flipped state;  $A_2O$  = open state;  $A_2D$  and  $A_2D'$  = desensitized states. This model was used for the  $\alpha_1$ L300V mutant. (B) Exemplary model fits for recordings in the excised-patch configuration for (a) WT receptor and (b)  $\alpha_1$ L300V (c) full duration pulse and (d) zoomed on the onset phase. To improve visibility, current traces for the WT receptors are drawn with a light gray line instead of a black one, as in part C. (C) Normalized simulated traces for WT and the  $\alpha_1$ L300V mutant generated for the mean values of the rate constants presented in part D in the  $\sim 1000$  ms time window. (D) Results of modeling presented in the same manner as in that in Figure 4D, including additional  $d_2'$  and  $r_2'$  rates.

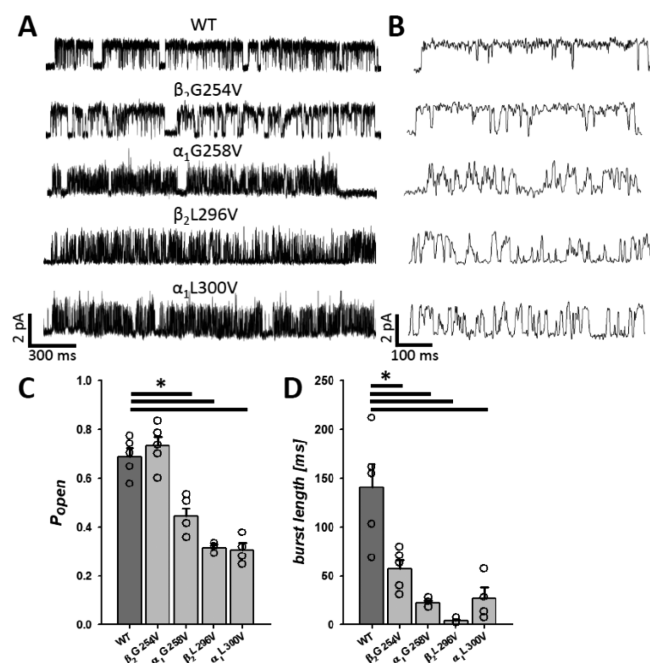
the WT receptors except for the time constant and percentage of the slow component ( $\tau_{\text{slow}}$  and  $\%A_{\text{slow}}$ , Table 1). In this situation, the strategy to implement the simplified model (Figure 4A) to fit the time course of responses within a limited time window (as in the case of the  $\alpha_1$ G258V and  $\beta_2$ L296V mutations) could not be applied. Thus, the extended model with two desensitized states had to be used (Figure 5A). In the fitting with the extended model, we considered the entire trace of current mediated by the  $\alpha_1$ L300V mutant with the slow desensitization phase and deactivation which also differed from that in the WT receptor mediated currents. Fitting of the entire trace with the extended model was somehow problematic, especially when starting the optimization procedure with initial guessing values for the rate constants distant from the optimized ones. Finally, it was possible to find a set of the optimized rate constants for each considered trace (exemplary fits for WT and the mutant in Figure 5Ba–d), but the initial guesses had to be set very close to the optimized values, otherwise either no convergence was observed or a non-reproducible variable and often extreme values of the rate constants were obtained. Although, at the end, we managed to collect the statistics for the model fitting for this mutant (see

Figure 5C for simulated traces), but we judge this set of fits as relatively poor, even if each individual fit fairly reproduced the time course of the current response. As shown in Figure 5D, in the  $\alpha_1$ L300V mutant, the three desensitization rates  $d_2$ ,  $d_2'$ , and  $r_2'$  were significantly reduced compared to those of the WT receptors, but the  $r_2$  rate was not affected by the mutation. Similar to those of the  $\alpha_1$ G258V and  $\beta_2$ L296V mutations, the opening rate  $\beta_2$  was strongly reduced in the mutant, but the closing rate  $\alpha_2$  was not significantly affected (note particularly large scatter for this rate constant). Finally, the preactivation (flipping) rate  $\delta_2$  was unaffected in  $\beta_2$ L300V, but contrary to the  $\alpha_1$ G258V and  $\beta_2$ L296V mutants, the unflipping rate  $\gamma_2$  was significantly reduced. In Figure 5C, we show simulated current responses for WT and the  $\beta_2$ L300V mutant for the mean values of the rate constants presented in Figure 5D.

Because of low activity, for the  $\beta_2$ G254V mutant, current responses were collected in the whole-cell configuration, and for the sake of comparison, controls for the WT receptors were recorded in the same conditions; a new modeling was done for these data. The rates for WT and the mutant were estimated in the same manner as that for  $\alpha_1$ G258V and  $\beta_2$ L296V, using the model with a single desensitized state (Figure 4A) and for the

~30 ms fitting time window (see Figure 4Bd,e). In these conditions, the temporal resolution is markedly smaller than that for recordings from excised-patches, and this might explain a large data scatter for the rate constants estimated in modeling (Figure 4Db). Nevertheless, the models could be accurately fitted to experimental traces, allowing to assess the impact of this mutation on conformational transitions. The only significant changes were found for  $d_2$  (increased) and  $r_2$  (decreased), in agreement with generally stronger macroscopic desensitization observed in this mutant. Changes of other rates were not statistically significant. Figure 4Cb shows simulated current responses for WT and the  $\beta_2$ G254V mutant for the mean values of the rate constants presented in Figure 4Db.

**Single-Channel Activity Reveals Major Changes in Gating Properties of the  $\alpha_1$ G258V,  $\alpha_1$ L300V, and  $\beta_2$ L296V Mutated Receptors.** To more precisely investigate effects of the mutations on the GABA<sub>A</sub>R activity, especially taking into account that modeling of macroscopic data was not particularly precise for some of the mutants, the analysis of single-channel currents elicited by saturating [GABA] (10 mM GABA) was performed. This analysis was focused on the predominant mode of activity for each considered mutant (see Materials and Methods). The difference between single-channel activity mediated by the  $\alpha_1$ G258V,  $\alpha_1$ L300V and  $\beta_2$ L296V mutants and the WT receptors was immediately apparent when just looking at the traces (Figure 6A,B). However, in the case of  $\beta_2$ G254V, the phenotype of activity similar to that of the WT receptors could be noticed (Figure 6A,B). Burst analysis (see Materials and Methods) revealed



**Figure 6.** Single-channel activity reveals diversified effects of mutations on activity patterns, burst lengths, and open probabilities. (A) Examples of typical clusters of single-channel activity (the predominant mode, see Materials and Methods) for the respective mutants and the WT receptors, showing marked changes in patterns of channel opening and closing. (B) Same as in part A but in expanded time scale. (C) Statistics for mean open probability ( $P_{open}$ ) calculated for bursts. (D) Statistics for the mean burst length. Note that these values are significantly shortened with respect to the WT receptors for all of the mutants.

that, for each considered mutant, except for  $\beta_2$ G254V, a strong reduction in the open probability ( $P_{open}$ ) took place ( $P_{open}$  for WT:  $0.69 \pm 0.04$ ,  $n = 5$ ; for  $\beta_2$ G254V:  $0.73 \pm 0.04$ ,  $n = 5$ ; for  $\alpha_1$ G258V:  $0.45 \pm 0.03$ ,  $n = 5$ ,  $p < 0.001$ ; for  $\beta_2$ L296V:  $0.32 \pm 0.01$ ,  $n = 3$ ,  $p < 0.001$ ; for  $\alpha_1$ L300V:  $0.31 \pm 0.03$ ,  $n = 4$ ,  $p < 0.001$ ; Figure 6C). However, all of the mutations, including  $\beta_2$ G254V, caused a large reduction of the mean burst length (for WT:  $140.29 \pm 24.78$  ms,  $n = 5$ ; for  $\beta_2$ G254V:  $57.32 \pm 9.27$  ms,  $n = 5$ ,  $p = 0.014$ ; for  $\alpha_1$ G258V:  $22.27 \pm 2.41$  ms,  $n = 4$ ,  $p = 0.016$ ; for  $\beta_2$ L296V:  $4.24 \pm 1.82$  ms,  $n = 3$ ,  $p = 0.006$ ; for  $\alpha_1$ L300V:  $27.06 \pm 11.27$  ms,  $n = 4$ ,  $p = 0.007$ ; Figure 6D).

Next, the dwell time distributions for closings and openings were analyzed. Shut time distributions for the WT receptors consisted of four components (at 40–80  $\mu$ s resolution), and the same number of components was found for  $\beta_2$ G254V. For all of the remaining mutants, only three components were needed. In the case of open times, two components (at 30–90  $\mu$ s resolution) were consistently detected in all of the considered cases. Typical examples of fitted distributions for shut and open times are shown in Figure 7. The statistics for shut time distributions are presented in Table 2. Because in the case of the  $\alpha_1$ G258V,  $\beta_2$ L296V and  $\alpha_1$ L300V mutations only three shut times components were present, the comparison to WT was done for the three shortest components. This strategy seems justified, as the time constant of the slowest, fourth component for the WT receptors was by far larger than any of those in the mutants.

As expected from the appearance of the single-channel traces and the exemplary shut time distribution (Figures 6 and 7), the impact of the  $\beta_2$ G254V mutation was rather weak: the only difference compared to WT was a decrease in the percentage of the second component ( $\%P_2$ , Table 2). However, the  $\alpha_1$ G258V,  $\beta_2$ L296V and  $\alpha_1$ L300V mutations profoundly altered the shut time distributions by not only affecting the number of components but also by dramatically altering the respective parameters. Most notably, typical shut time distributions for these mutants (Figure 7) showed a dramatic reduction in the bin content for the short-lasting closures. Indeed, in the case of these mutants, the shortest time constant ( $\tau_1$ ) is markedly increased and its percentage ( $\%P_1$ ) is strongly reduced. Moreover, in the case of the second component, both the time constant ( $\tau_2$ ) and its percentage ( $\%P_2$ ) are markedly increased. These alterations in the two shortest shut time components reveal an overall robust increase in the short closure duration, indicative for a strong reduction of the opening rate of the receptor. Moreover, in the case of  $\beta_2$ L296V, the percentage of the third component ( $\%P_3$ ) was slightly increased.

Time constants and percentages for the components present in the distributions for the WT receptors and  $\beta_2$ G254V,  $\alpha_1$ G258V,  $\alpha_1$ L300V and  $\beta_2$ L296V mutants: without brackets = experimental parameters; normal brackets = simulated with experimental resolution; square brackets = simulated with 0  $\mu$ s resolution. Statistically significant changes relative to WT are highlighted in bold with an asterisk (\*) and the corresponding  $p$  value;  $n$  = number of patches.

To complete our analysis of dwell time distributions, open times were investigated (Figure 7; Table 3). The  $\beta_2$ G254V mutation did not affect the open times significantly, which further confirmed its similarity to the WT phenotype. However, in the rest of the mutants, a clear trend of shortening of opening was observed. Indeed, in  $\alpha_1$ G258V, the percentage of the fastest component ( $\%P_1$ ) was significantly increased

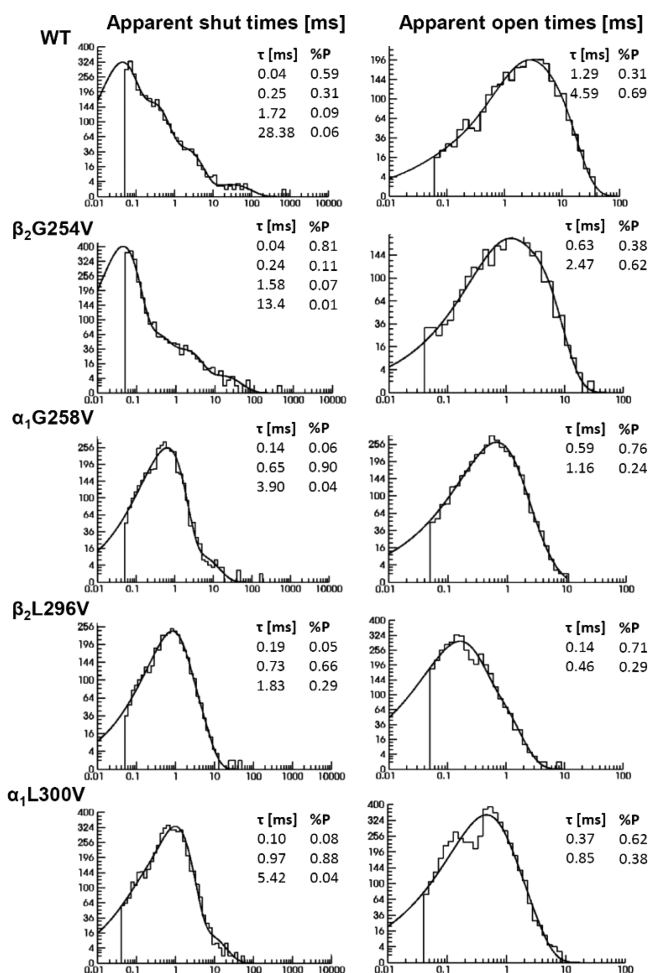


**Figure 7.** Distributions of apparent shut and open times for WT and the  $\beta_2$ G254V,  $\alpha_1$ G258V,  $\alpha_1$ L300V and  $\beta_2$ L296V mutants indicate major changes in gating properties. Examples of typical dwell time distributions for shut times (left panel) and open times (right panel) that were fitted with probability density functions and the respective parameters of each component (time constant  $\tau$  and its percentage %P) are presented in insets. In shut time distributions for WT and  $\beta_2$ G254V, four components are present, while for the  $\alpha_1$ G258V,  $\alpha_1$ L300V and  $\beta_2$ L296V mutants, there are only three. For statistics, see Table 2 (shut times) and Table 3 (open times).

(with concomitant decrease in percentage of slower component %P<sub>2</sub>), whereas in the case of  $\beta_2$ L296V and  $\alpha_1$ L300V, both open time constants ( $\tau_1$  and  $\tau_2$ ) were significantly shortened (Table 3). Based on the distribution parameters, mean (weighted) open times (%P<sub>1</sub> $\tau_1$  + %P<sub>2</sub> $\tau_2$ ) were calculated, and for the  $\alpha_1$ G258V,  $\alpha_1$ L300V and  $\beta_2$ L296V mutants this value was significantly reduced compared to that of WT (Table 3). Notably, in the case of  $\beta_2$ L296V, mean open time was shortened by nearly 1 order of magnitude, indicating a particularly strong impact on the closing transition. Taken together, except for the  $\beta_2$ G254V mutation, which did not affect single-channel openings in all the remaining mutants, an overall trend to shorten the open times was observed, suggesting an increased closing rate compared to that of the WT receptors.

Time constants and the percentages of the two open time components and mean open time for the WT,  $\beta_2$ G254V,  $\alpha_1$ G258V,  $\alpha_1$ L300V and  $\beta_2$ L296V receptors: without brackets = experimental parameters; normal brackets = simulated with

experimental resolution; square brackets = simulated with 0  $\mu$ s resolution. Statistically significant changes relative to WT are highlighted in bold with an asterisk (\*) and the corresponding *p* value; *n* = number of patches.

**Kinetic Modeling of Single-Channel Data.** Having detected single-channel events and characterized the dwell time distributions (Tables 2 and 3), we used HJCFIT software to perform modeling of the single-channel data. Because all of the receptors had two components in open time distributions, in all models, two open states were included. Also because the WT receptors and the  $\beta_2$ G254V mutant had shut time distributions consisting of four components, the extended model from Kisiel et al.<sup>23</sup> with four shut states (one closed, one preactivated, and two desensitized states) was employed (Figure 8A). Consistently, in the case of the  $\alpha_1$ G258V,  $\alpha_1$ L300V and  $\beta_2$ L296V mutants, three shut states (one desensitized state only) were included in the model (Figure 8B). These model schemes for gating are more complex than the ones used in the macroscopic modeling (Figures 4 and 5), but as pointed out by Colquhoun and Lape,<sup>31</sup> the single-channel modeling is less susceptible to model overparametrization than the macroscopic one. Clearly, because the recordings were carried out in the stationary conditions in the presence of saturating [GABA], the binding steps in the schemes were omitted.

Model fitting for the  $\beta_2$ G254V mutant generally confirmed that its kinetic phenotype was similar to that of the WT receptors, although some relatively minor differences were found. Specifically, the flipping and unflipping rates  $\delta_2$  and  $\gamma_2$ , were slightly (but significantly) reduced and also, the rates describing desensitization ( $r_2$  and  $d_2$ ) were altered indicating enhancement of desensitization (Figure 8D) which corroborates our macroscopic findings.

Upon applying the optimization procedures to fit the selected models to the data collected for the  $\alpha_1$ G258V,  $\alpha_1$ L300V and  $\beta_2$ L296V mutants, we encountered a technical problem. Because of a very small percentage of one of the components (the shut fastest one), the HJCFIT fitting algorithm either failed to converge or tended to yield extreme (and largely random in successive trials) values of the rate constants, especially for the preactivation parameters ( $\delta_2$  and  $\gamma_2$ ). In order to bypass this problem, we performed the optimization in two stages. First, we simplified the distribution by subtracting the slowest shut component using the critical time ( $t_{crit}$ ) criterion.<sup>32</sup> This choice was made based on consideration of the fact that the slowest component for the intracuster events is attributed to the desensitization transitions<sup>23</sup> and therefore, the data for such a “truncated” shut time distribution were fitted with a simplified model without the desensitized state (Figure 8C). In these conditions, the fit was highly reproducible. Then, such obtained rate constants  $\delta_2$  and  $\gamma_2$  were fixed and used in fitting to the full model (Figure 8B) to the complete data (with entire shut times distributions). Fitting of the full data with the complete model with fixed  $\delta_2$  and  $\gamma_2$  rates was successful and reproducible. The reliability of this two-step procedure was ultimately validated by confronting the theoretical distributions generated with this modeling with the experimental ones, and as shown in Figure 8E, these distributions overlapped very well. Moreover, when confronting results of such two-step modeling for the WT receptors with data obtained using one-step fitting (Figure 8D), the values of optimized rate constants



Table 2. Mean Values of Parameters of Shut Time Distributions

shut time	$\tau_1$ [ms]	%P <sub>1</sub>	$\tau_2$ [ms]	%P <sub>2</sub>	$\tau_3$ [ms]	%P <sub>3</sub>	$\tau_4$ [ms]	%P <sub>4</sub>
WT <i>n</i> = 5	0.04 ± 0.003 (0.06 ± 0.01) [0.05 ± 0.01]	0.57 ± 0.03 (0.45 ± 0.05) [0.51 ± 0.03]	0.26 ± 0.01 (0.34 ± 0.02) [0.32 ± 0.02]	0.32 ± 0.02 (0.38 ± 0.05) [0.35 ± 0.04]	1.55 ± 0.11 (1.70 ± 0.17) [1.68 ± 0.17]	0.10 ± 0.01 (0.16 ± 0.02) [0.13 ± 0.02]	20.42 ± 2.71 (20.95 ± 3.03) [20.94 ± 3.03]	0.01 ± 0.002 (0.01 ± 0.002) [0.01 ± 0.001]
$\beta_2$ G254V <i>n</i> = 5	0.05 ± 0.01 (0.06 ± 0.01) [0.06 ± 0.01]	0.68 ± 0.05 (0.57 ± 0.04) [0.61 ± 0.04]	0.36 ± 0.05 (0.50 ± 0.02) [0.49 ± 0.02]	<b>0.17 ± 0.02*</b> <i>p</i> < 0.001 (0.25 ± 0.03) [0.23 ± 0.03]	<b>2.26 ± 0.28*</b> <i>p</i> = 0.043 (2.63 ± 0.35) [2.61 ± 0.35]	0.10 ± 0.02 (0.15 ± 0.03) [0.13 ± 0.03]	19.25 ± 3.70 (18.35 ± 3.35) [18.31 ± 3.85]	<b>0.04 ± 0.01*</b> <i>p</i> = 0.038 (0.04 ± 0.02) [0.03 ± 0.01]
$\alpha_1$ G258V <i>n</i> = 5	<b>0.23 ± 0.04*</b> <i>p</i> = 0.008 (0.21 ± 0.05) [0.20 ± 0.05]	<b>0.08 ± 0.02*</b> <i>p</i> < 0.001 (0.12 ± 0.04) [0.17 ± 0.05]	<b>0.85 ± 0.06*</b> <i>p</i> = 0.008 (0.89 ± 0.07) [0.76 ± 0.07]	<b>0.87 ± 0.01*</b> <i>p</i> < 0.001 (0.83 ± 0.03) [0.79 ± 0.04]	<b>3.41 ± 0.32*</b> <i>p</i> < 0.001 (3.84 ± 0.88) [3.82 ± 0.81]	<b>0.05 ± 0.01*</b> <i>p</i> = 0.038 (0.05 ± 0.01) [0.04 ± 0.01]		
$\beta_2$ L296V <i>n</i> = 3	<b>0.19 ± 0.03*</b> <i>p</i> = 0.036 (0.10 ± 0.01) [0.09 ± 0.01]	<b>0.08 ± 0.04*</b> <i>p</i> < 0.001 (0.10 ± 0.02) [0.16 ± 0.02]	<b>0.88 ± 0.12*</b> <i>p</i> < 0.001 (0.96 ± 0.16) [0.73 ± 0.11]	<b>0.69 ± 0.07*</b> <i>p</i> < 0.001 (0.74 ± 0.06) [0.76 ± 0.05]	<b>2.24 ± 0.32*</b> <i>p</i> = 0.043 (2.61 ± 0.42) [2.51 ± 0.44]	<b>0.22 ± 0.04*</b> <i>p</i> = 0.015 (0.16 ± 0.07) [0.09 ± 0.03]		
$\alpha_1$ L300V <i>n</i> = 4	<b>0.11 ± 0.02*</b> <i>p</i> = 0.005 (0.11 ± 0.005) [0.11 ± 0.004]	<b>0.05 ± 0.01*</b> <i>p</i> < 0.001 (0.06 ± 0.02) [0.08 ± 0.02]	<b>1.08 ± 0.05*</b> <i>p</i> = 0.016 (1.07 ± 0.05) [0.86 ± 0.03]	<b>0.87 ± 0.03*</b> <i>p</i> = 0.036 (0.85 ± 0.04) [0.86 ± 0.03]	<b>4.75 ± 0.83*</b> <i>p</i> = 0.016 (4.22 ± 0.58) [4.16 ± 0.60]	0.08 ± 0.03 (0.09 ± 0.03) [0.05 ± 0.01]		

Table 3. Mean Values of Parameters of Open Time Distribution

open time	$\tau_1$ [ms]	%P <sub>1</sub>	$\tau_2$ [ms]	%P <sub>2</sub>	mean open time [ms]
WT <i>n</i> = 5	1.02 ± 0.14 (0.90 ± 0.10) [0.57 ± 0.05]	0.55 ± 0.08 (0.87 ± 0.04) [0.94 ± 0.02]	2.86 ± 0.49 (2.90 ± 0.56) [2.77 ± 0.53]	0.45 ± 0.08 (0.13 ± 0.04) [0.06 ± 0.02]	1.92 ± 0.42 (1.16 ± 0.17) [0.69 ± 0.08]
$\beta_2$ G254V <i>n</i> = 5	0.88 ± 0.26 (0.99 ± 0.21) [0.64 ± 0.14]	0.42 ± 0.06 (0.81 ± 0.04) [0.8 ± 0.04]	3.06 ± 0.82 (3.84 ± 0.62) [3.62 ± 0.61]	0.58 ± 0.07 (0.19 ± 0.04) [0.11 ± 0.04]	2.22 ± 0.60 (1.51 ± 0.23) [0.95 ± 0.16]
$\alpha_1$ G258V <i>n</i> = 5	<b>0.55 ± 0.09*</b> <i>p</i> = 0.019 (0.47 ± 0.09) [0.42 ± 0.09]	<b>0.82 ± 0.04*</b> <i>p</i> = 0.016 (0.80 ± 0.03) [0.84 ± 0.02]	<b>1.39 ± 0.28*</b> <i>p</i> = 0.031 (1.22 ± 0.30) [1.19 ± 0.30]	<b>0.18 ± 0.04*</b> <i>p</i> = 0.016 (0.20 ± 0.03) [0.16 ± 0.02]	<b>0.68 ± 0.10*</b> <i>p</i> = 0.008 (0.60 ± 0.10) [0.58 ± 0.14]
$\beta_2$ L296V <i>n</i> = 3	<b>0.12 ± 0.001*</b> <i>p</i> = 0.003 (0.12 ± 0.01) [0.11 ± 0.01]	0.57 ± 0.03 (0.62 ± 0.05) [0.72 ± 0.05]	<b>0.52 ± 0.04*</b> <i>p</i> = 0.011 (0.47 ± 0.04) [0.45 ± 0.04]	0.42 ± 0.04 (0.33 ± 0.05) [0.28 ± 0.05]	<b>0.26 ± 0.03*</b> <i>p</i> = 0.036 (0.24 ± 0.03) [0.21 ± 0.03]
$\alpha_1$ L300V <i>n</i> = 4	<b>0.20 ± 0.07*</b> <i>p</i> = 0.002 (0.20 ± 0.07) [0.19 ± 0.06]	0.52 ± 0.12 (0.56 ± 0.12) [0.60 ± 0.12]	<b>0.62 ± 0.11*</b> <i>p</i> = 0.005 (0.61 ± 0.12) [0.59 ± 0.12]	0.48 ± 0.12 (0.44 ± 0.12) [0.40 ± 0.12]	<b>0.39 ± 0.06*</b> <i>p</i> = 0.016 (0.36 ± 0.05) [0.33 ± 0.05]

were statistically indistinguishable (data not shown), further confirming the validity of the two-step approach.

In the case of the  $\alpha_1$ G258V mutant, the flipping rate  $\delta_2$  was unaltered compared to that of the WT receptors, but unflipping  $\gamma_2$  was significantly reduced (Figure 8D). In contrast, in the case of the  $\beta_2$ L296V and  $\alpha_1$ L300V mutants, no significant changes in the preactivation rate constants ( $\delta_2$  and  $\gamma_2$ ) were found. In both  $\alpha_1$ G258V and  $\beta_2$ L296V mutants the opening ( $\beta_2$  and  $\beta_2'$ ) rates were strongly reduced, while the closing rates ( $\alpha_2$  and  $\alpha_2'$ ) were markedly upregulated (Figure 8D). These results on the opening and closing rates appear compatible with particularly evident shortenings of the single-channel openings and prolongation of closures (Figure 7, Tables 2 and 3). Moreover, in these two mutants, a decrease in the desensitization rate  $d_2$  was observed compared to that of WT (Figure 8D) which is in qualitative agreement with

weakening of the macroscopic desensitization in these mutants (Figure 3 and Table 1). Taken altogether, the single-channel data modeling revealed two qualitatively different phenotypes: In the case of  $\alpha_1$ G258V,  $\alpha_1$ L300V and  $\beta_2$ L296V mutations, the predominant effects were weakening of desensitization combined with a strong impairment of opening/closing transitions, whereas for the  $\beta_2$ G254V mutation, an upregulated desensitization and a moderately affected preactivation were observed.

**Where Is Desensitization Transition Originating from? Bifurcating (Figure 4A) vs Linear Model.** The fact that the activation and desensitization gates are located in the close neighborhood on the M2 pore lining segment might suggest that desensitization could originate from the open conformation. This scenario would convert our model from a bifurcating one (Figure 4Aa) to the linear one ( $R \leftrightarrow AR \leftrightarrow$

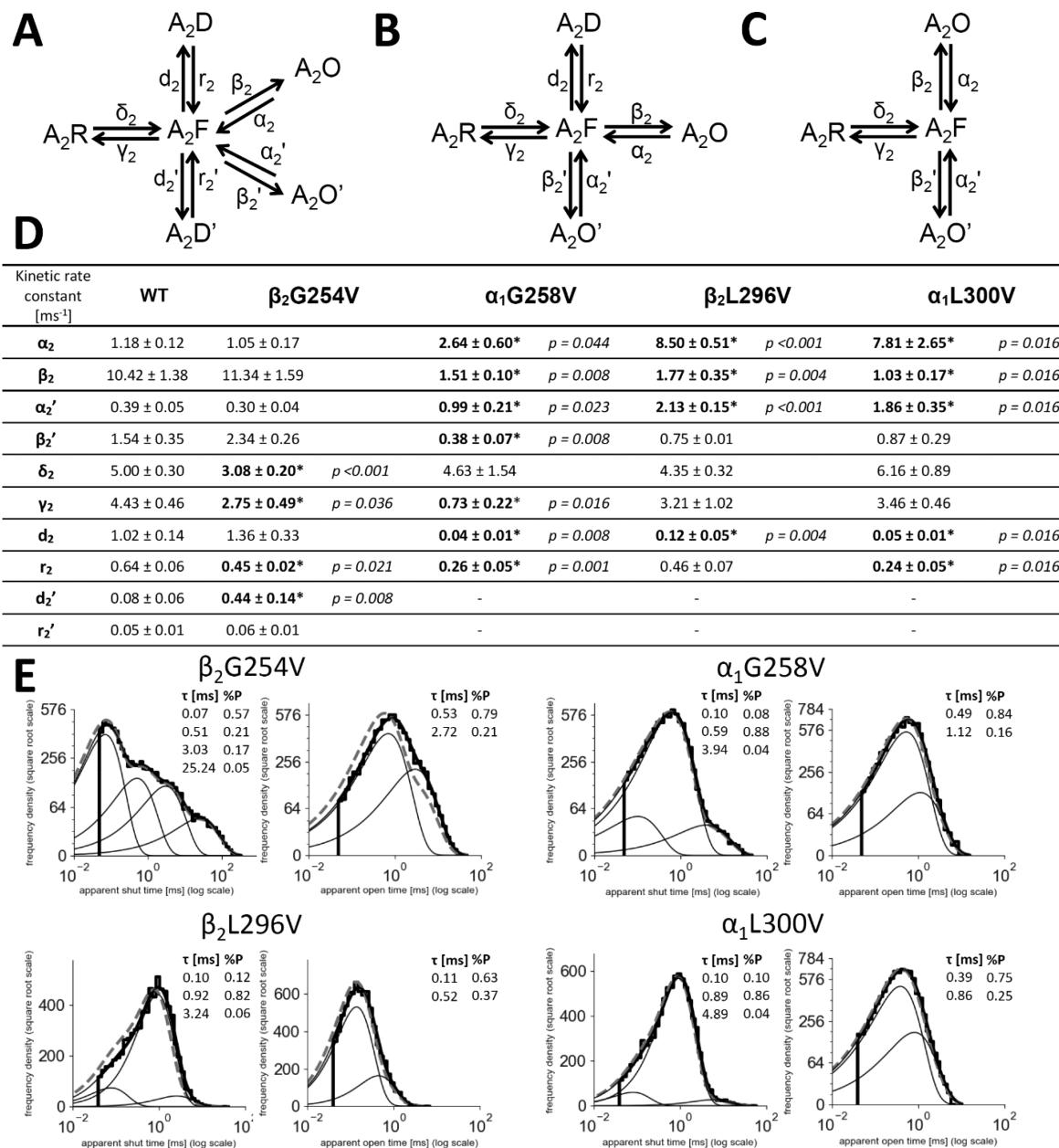


**Figure 8.** Results of the single-channel modeling reveal major changes caused by the  $\alpha_1$ G258V,  $\alpha_1$ L300V and  $\beta_2$ L296V mutations on opening, closing and desensitization rates but only a minor effect on preactivation. (A) Scheme of the full kinetic model from Kisiel et al.<sup>23</sup> with two open and two desensitized states that was used for modeling of the WT and  $\beta_2$ G254V receptors. In the scheme:  $A_2R$  = doubly bound receptor;  $A_2F$  = flipped state;  $A_2O$  and  $A_2O'$  = open states;  $A_2D$  and  $A_2D'$  = desensitized states. (B) The same model as that in part A but with one desensitized state ( $A_2D$ ). This model was used for modeling of the mutants with only three shut time components ( $\alpha_1$ G258V,  $\alpha_1$ L300V and  $\beta_2$ L296V). (C) A scheme of a kinetic model with only two closed ( $A_2R$  and  $A_2F$ ) and two open ( $A_2O$  and  $A_2O'$ ) states and no desensitization, which was used in the intermediate step of modeling for the  $\alpha_1$ G258V,  $\alpha_1$ L300V and  $\beta_2$ L296V mutants (see single-channel modeling section). (D) Results of modeling presented in the table as mean values of the kinetic rate constants for each gating transition for the considered mutants. Significant changes in the rate constants vs WT are marked in bold with an asterisk (\*), and the corresponding  $p$  value is disclosed. (E) Solid black lines present examples of the simulated dwell time distributions of the frequency density functions overlaid on the experimental shut and open time distributions (insets present time constants  $\tau$  and percentages %P of the components present in the simulated distributions). Solid gray, thin lines outline the exponential components in apparent shut and open time distributions. Gray, thick, dashed lines show the distributions obtained with an application of the corrections for missed events.

$A_2R \leftrightarrow A_2F \leftrightarrow A_2O \leftrightarrow A_2D$ , referred to as the flipped linear model, fLM). To check this possibility, we have tentatively re-examined our modeling for  $\alpha_1$ G258V and  $\beta_2$ L296V mutants, for which the effects were very clear, both at the macroscopic and single-channel levels using these two simplified schemes. Both models allowed to fairly fit the time course of the current responses mediated by WT and the mutated receptors.

However, whereas the bifurcating model (Figure 4Aa) well-reproduced the mean open time for the WT receptors (calculated as  $1/\alpha_2$ , 0.85 ms), for fLM, it was 0.38 ms (calculated as  $1/(\alpha_2 + d_2)$ ) which is much shorter than that determined in the experiment (Table 3). Moreover, the most disappointing was the estimation of the mean open time using the fLM model for the mutants: 0.54 and 1.73 ms for  $\alpha_1$ G258V

and  $\beta_2$ L296V, respectively, i.e., markedly longer than for the WT receptors (0.38 ms) estimated for this model which is in sharp contrast with that of the experiment (Table 3). At the same time, the bifurcating model (Figure 4Aa) correctly reproduced shortening of the mean open time for these mutants. This analysis confirms the validity of the bifurcating model (Figure 4Aa), thus reinforcing the notion that the desensitization transition occurs from the intermediate (preactivated/flipped) state rather than from the open conformation.

**Role of the Second and Third Transmembrane Domains Is Not Limited to Desensitization.** In the present report we addressed the impact of the mutations localized at the second and third transmembrane domains, close to their intracellular ends. This region was indicated by Gielen et al.<sup>27</sup> as the desensitization gate and the mutations considered here were also explored by these authors. Our most important finding is that, although the  $\alpha_1$ G258V,  $\alpha_1$ L300V,  $\beta_2$ L296V and  $\beta_2$ G254V mutations did affect desensitization, their impact was not specific for this transition. In the cases of the  $\alpha_1$ G258V,  $\alpha_1$ L300V and  $\beta_2$ L296V mutants, there was additionally a very strong effect on opening/closing and, in the case of  $\alpha_1$ G258V and  $\beta_2$ G254V, a relatively minor effect on the preactivation transition. In addition to these effects on the receptor gating, we observed only a moderate impact on the agonist potency suggesting a weak effect on the agonist binding step. Thus, our results point to a general conclusion that mutations in this region affect late conformational transitions including opening/closing and desensitization with relatively minor effects on preactivation and agonist binding. Thus, in reference to the desensitization process, our results and those of Gielen et al.<sup>27</sup> are in agreement, but our study extends previous findings by providing further evidence that structural determinants for various conformational transitions are intermingled and tend not to be compartmentalized.

While drawing the comparison to the study of Gielen et al.,<sup>27</sup> it is also important to indicate crucial methodological differences with respect to the present study. Most of the data presented by this group concerns GABA<sub>A</sub>  $\alpha_1\beta_2$  receptors (there is also a comparative set of data on  $\alpha_1\beta_2\gamma_2$  receptors and glycine receptors), while our report is dedicated exclusively to  $\alpha_1\beta_2\gamma_2$  receptors. In our hands, expression of  $\alpha_1\beta_2$  receptors was much smaller than those containing the  $\gamma_2$  subunit which would preclude single-channel recordings. Gielen et al.<sup>27</sup> based their reasoning on observations of the macroscopic desensitization, whereas in our study, the rate constants for microscopic desensitization ( $d_2$ ,  $r_2$ ) and for the other transitions (opening/closing and preactivation) were extracted from the macroscopic and single-channel recordings and modeling. As correctly pointed out by these authors, changes induced by the mutations might affect gating efficacy and thereby influence the macroscopic desensitization without actually modifying the microscopic desensitization rates. In general, a precise determination of how a considered mutation affects a specific gating property is difficult, because any kinetic feature of the recorded current responses (e.g., macroscopic desensitization, rise time, or deactivation) may depend on all of the rate constants in the considered gating model.<sup>33–36</sup> In reference to the macroscopic desensitization, this issue was investigated in detail by our group in our study by Szczot et al.<sup>26</sup> (see Figure 10 in this reference) and also by Macdonald and co-workers.<sup>37</sup> Most of the studies carried out by Gielen et al.<sup>27</sup> were performed on oocytes (although a set of comparative

recordings in HEK 293 cells was also presented) with a slow solution exchange, whereas in our study, rapid solution “jumps” were used; therefore, it is possible that different components of the receptor gating (especially for desensitization) were observed. An important difference was also that Gielen et al.<sup>27</sup> implemented a wide spectrum of mutation strategies, including chimeras with various portions of different subunit types as well as pairs of point mutations. This elegant approach offered them an advantage to consider potential interactions between specific localizations, e.g., between the M2 and M3 transmembrane segments, and most data presented in their report concerns either double mutants or chimeric structures. In our report, we considered single substitutions which yielded a clear change in kinetic phenotype, and we focused on precise determination of alterations in gating properties by applying macroscopic and single-channel analysis. The use of these two options of recordings offered an advantage to base our inferences on the complementary analyses which, taken together, reinforced our conclusions. It needs to be mentioned, however, that there were some relatively minor discrepancies in assessment of the gating rate constants from the macroscopic and single-channel data. Not surprisingly, the estimation of the desensitization rate constants ( $d_2$ ,  $r_2$ ) from macroscopic nonstationary recordings differed from that based on stationary single-channel measurements for all of the tested receptors. As extensively discussed in our previous reports, the desensitization onset can be clearly observed upon rapid agonist applications, offering a unique opportunity to characterize respective rate constants, whereas in the stationary recordings, this dynamic phase of the desensitization process is not visible; therefore, the reliability of estimation of the desensitization rates is limited.<sup>21,38</sup> Nevertheless, in the single-channel modeling we reproduced well, at the qualitative level, changes in desensitization observed in the macroscopic recordings (for  $\alpha_1$ G258V,  $\alpha_1$ L300V,  $\beta_2$ L296V = reduction of desensitization and for  $\beta_2$ G254V = enhancement). For the  $\alpha_1$ G258V and  $\alpha_1$ L300V mutants, the lack of effect on the flipping rate  $\delta_2$  was consistent in the macroscopic and single-channel modeling, but there were differences for the unflipping rate  $\gamma_2$  (Figures 4, 5, and 8). In addition, for  $\beta_2$ G254V, both  $\delta_2$  and  $\gamma_2$  were reduced in the single-channel modeling, and this effect was not confirmed in the macroscopic analysis. The reason for these discrepancies is likely to be related, at least to some extent, to different recording conditions but also to the fact that the macroscopic modeling for extensive models is probably more problematic than that based on the single-channel recordings. Nevertheless, it needs to be stressed that our key conclusions indicating major effects of these mutations on the desensitization and opening/closing transitions are particularly consistent in the two approaches.

It is of note that in our study the  $\alpha_1$ G258V mutation was found to reduce the macroscopic desensitization, while Gielen et al.,<sup>27</sup> who studied this substitution together with other mutations (e.g.,  $\beta_2$ G254A), reported desensitization acceleration and its increased extent. Most likely these different observations reflect the distinct functional impact of a single and double mutations. On the other hand, the  $\beta_2$ G254V mutation enhanced desensitization in our experiments, similar to observations by Gielen et al.<sup>27</sup> Thus, taken altogether, our data are in agreement with those of Gielen et al.,<sup>27</sup> where the M2 and M3 transmembrane segments play an important role in the mechanisms underlying the desensitization process. The

importance of the M2 transmembrane segment (but also of M1) was also emphasized by Bianchi and Macdonald<sup>39</sup> who considered the GABA<sub>A</sub> receptor chimeras containing portions of  $\gamma 2$  and  $\delta$  subunits when examining the structural determinants of various slow and fast desensitization components. The major novelty brought by our present study is that the considered residues in the M2 and M3 transmembrane segments, besides being involved in desensitization, have a nearly equally strong impact on the opening/closing transitions. This finding is not surprising as the presumed opening and desensitization restriction gates within the channel pore are not distant from each other<sup>14,40</sup> (Figure 1C).

**Structural Determinants of Desensitization, Emerging Concept of Diffuse Gating Mechanism.** The major point that, in our opinion, deserves a particular emphasis, is that the region of M2 and M3 segments is not unique for determining either opening/closing (“efficacy”) or desensitization. Several studies by our group and by others clearly indicated that the mutations located close to the agonist binding site may have a strong impact on receptor gating, including the specific effect on efficacy:  $\beta_2$ F200 (loop C),<sup>24</sup>  $\alpha_1$ F45 (loop G),<sup>22</sup>  $\alpha_1$ F64A (loop D),<sup>38</sup>  $\beta_2$ E155 (loop B).<sup>25,41</sup> Another intriguing consequence of the mutations at the proximity of the GABA<sub>A</sub> agonist binding sites is increased spontaneous activity, further underscoring long-range structural interactions underlying receptor openings (e.g.,  $\beta_2$ E155).<sup>25,28,41,42</sup> These observations clearly indicate that molecular mechanisms underlying receptor openings comprise not only the areas close to the channel opening gate but also several distant regions, which is best documented by involvement of areas close to the agonist binding sites.

The present study adds an interesting observation that structural elements lying “behind” the channel opening gate (from the viewpoint of LBS) are also strongly involved in the receptor opening/closing transitions. The major point that emerges from our present and previous data is that a similar conclusion concerning widespread gating also holds for structural determinants of the desensitization process. There is no doubt that the M2 and M3 transmembrane segments play an important role in determining GABA<sub>A</sub> desensitization, but several reports also indicate other structural determinants, practically in all major regions of this receptor. As already mentioned in the Introduction, mutation of the  $\alpha_1$ F45 residue (loop G)<sup>22</sup> affected practically all gating features of the receptor including preactivation, opening/closing, and desensitization providing another example that structural determinants for these gating transitions are shared. Similar conclusions were drawn in our recent study on the role of the loop C ( $\beta_2$ F200)<sup>24</sup> in which the impact on all gating characteristics, including desensitization, was reported. Perhaps the most surprising was our recent observation that the mutation of  $\alpha_1$ F14 and  $\beta_2$ F31 residues, located nearly at the “top” of the ECD, had again a clear impact on all gating transitions including desensitization.<sup>21</sup> Moreover, it was shown that the involvement of these residues in the receptor gating depends on intersubunit interactions mediated by these phenylalanine residues, further underscoring long-range interactions in the structural mechanisms underlying conformational transitions. All these observations point to the concept of “diffuse gating mechanism” for all conformational transitions, including desensitization. Clearly, some localizations within the GABA<sub>A</sub> receptor macromolecule might be

more critical than the others for various gating features. As comprehensively reviewed by e.g., Cederholm et al.<sup>1</sup> and Miller and Smart,<sup>2</sup> mutations of some residues, e.g. at the ECD-TMD interface are “lethal” for receptor gating, whereas others might rather play a “modulatory” role in shaping distinct gating features of this receptor. Nevertheless, the picture emerges that GABA<sub>A</sub> activation reflects cooperative actions based on several long-range interactions, and therefore, the molecular determinants of receptor gating need to be studied “holistically” by considering GABA<sub>A</sub> entire structure. It is important to add that Gielen and co-workers,<sup>27</sup> when proposing the localization of the “desensitization gate” at the M2 and M3 transmembrane segments, were aware of a possibility of widespread rearrangements of the GABA<sub>A</sub> macromolecule at the ECD-TMD interface and possibly in ECD, whose movement would be triggered by rigid-body motion of the M2 helices.

Based on structural data, clearly indicating two constriction sites at the channel pore<sup>14,40</sup> interpreted as the activation gate (between the 16' and 9' residues) and desensitization gate (around 2' residue), a concept of two-gate mechanism has been proposed.<sup>43</sup> However, recent data on  $\alpha_7$  homomeric nAChR<sup>44</sup> indicate that both gates might be related to the desensitized state. Our conclusions generally agree with this idea in the sense that final steps of the activation and desensitization conformational transitions are occurring at specific gates at the channel pore, but these processes, especially their preceding steps, are dependent on long-range interactions comprising vast parts of the receptor macromolecule, reflecting the concept of diffuse gating mechanisms.

It is worth mentioning that, in the case of the structurally related pentameric bacterial channel GLIC<sup>45</sup> as well as possibly GlyR<sup>46</sup> and nAChR,<sup>47</sup> a concerted counterclockwise movement comprising both ECD and TMD was demonstrated, nicely illustrating importance of long-range interactions eventually resulting in quaternary twist and tertiary deformation of these macromolecules.

**Mutations Probably Alter Primarily Interactions within TMD.** An important question that arises from our research concerns the molecular mechanisms underlying the effects of the considered point mutations on observed changes in the receptor's kinetic behavior. Although we have not performed either any in depth physicochemical analysis of altered interactions induced by the considered substitutions or molecular dynamics studies, we believe it is worthwhile to (speculatively) reflect on the nature of the possible underlying molecular scenarios. All of the investigated residues are located at the M2 (pore-lining) or M3 (located in the “inner ring” of the TMD helices bundle)  $\alpha$ -helices (Figure 1B). Considering that, on the M2 segment, both opening/closing and desensitization constriction sites are located, it seems unsurprising that changes in these kinetic characteristics are so strongly correlated in our mutagenesis studies. Apart from a possible influence of the mutated residues on general stability and conformation of the TMD helices, an interaction with the membrane cannot be excluded. However, the investigated region is located in the hydrophobic area (see the lack of charged residues in Figure 1C) and between tryptophan residues (often anchoring the protein in the membrane at the level of lipid head groups, Figure 1C). Thus, these hypothetical interactions would be limited to nonspecific, low energy couplings with lipid tails or other constituents of the membrane at the level of the membrane's inner leaflet. Thus,

the scenario that seems to be most probable is that observed effects of mutations are caused by changes of van der Waals interactions in the areas between the TMD helices, which ultimately alter the tightness of the helical bundles, thereby influencing their motions linked to gating, that takes the form of the twisting of the subunits and tightening of the pore.

In conclusion, we provide evidence that mutations of M2 and M3 in the TMD strongly affect late gating transitions including opening/closing and desensitization, only weakly changing preactivation and binding. These findings provide further support to the view that the molecular determinants of distinct conformational transitions are shared, and their molecular mechanisms are structurally widespread, pointing to a concept of diffuse gating of GABA<sub>A</sub>R.

## MATERIALS AND METHODS

**Cell Culture and Expression of Recombinant GABA<sub>A</sub>Rs.** All experiments were performed on HEK 293 cells (European Collection of Authenticated Cell Culture, Salisbury, UK) cultured in Dulbecco's Modified Eagle's Medium with 10% FBS and 1% Pen/Strep (Thermo Fisher Scientific, Waltham, MA, US) in a humidified atmosphere with 5% CO<sub>2</sub> at 37 °C. Cells were transferred from flasks and replated on Poly-D-lysine (1 μg/ml) coated coverslips (Carl Roth, Karlsruhe, Germany) and, after 24 h, transiently transfected with FuGENE HD transfection reagent (Promega, Madison, WI, US) at a 3:1 FuGENE HD:DNA ratio with adenoviral pCMV-based plasmids containing rat cDNA of GABA<sub>A</sub>R subunits. Both for wild-type and mutated receptors, the subunits ratio in the transfection solution was: 1:1:3 (0.5:0.5:1.5 μg) with added 0.5 μg of EGFP encoding plasmid for visualization of successfully transfected cells using the fluorescence illuminator (470 nm wavelength, CoolLED, Andover, UK) mounted on a modular inverted microscope (Leica DMi8, Wetzlar, Germany).

**Electrophysiology.** Patch-clamp recordings were performed 48 h after transfection. Macroscopic currents evoked by saturating GABA (10 mM) or nonsaturating solutions (for dose–response relationships only) were low-pass-filtered at 10 kHz and recorded at a holding potential of –40 mV using an Axopatch 200B amplifier (Molecular Devices, Sunnyvale, CA, US) and acquired using a Digidata 1550A acquisition card (Molecular Devices, Sunnyvale, CA, US). For signal acquisition, pClamp 10.7 software (Molecular Devices, Sunnyvale, CA, US) was used. Borosilicate glass pipettes (outer diameter = 1.5 mm; inner diameter = 1.0 mm; Hilgenberg, Malsfeld, Germany) were pulled using a P-97 horizontal puller (Sutter Instruments, Novato, CA, US) and filled with intracellular solution (mM): 137 KCl, 1 CaCl<sub>2</sub>, 2 ATP-Mg, 2 MgCl<sub>2</sub>, 10 K-gluconate, 11 EGTA, and 10 HEPES, with the pH adjusted to 7.2 with KOH. The resistance of the pipettes filled with the internal solution were in the range 3–5 MΩ. As the external saline, Standard Ringer's solution was used (mM): 137 NaCl, 5 KCl, 2 CaCl<sub>2</sub>, 1 MgCl<sub>2</sub>, 10 HEPES, and 20 glucose, with the pH adjusted to 7.2 with NaOH and the osmolarity adjusted to ~320 mOsm with glucose. Currents were evoked from outside-out membrane patches or in the whole-cell configuration (lifted-cell mode) with the ultrafast perfusion system based on a two-channel θ-glass capillary (Hilgenberg, Malsfeld, Germany) mounted on a piezoelectric-driven translator (Physik Instrumente, Karlsruhe, Germany), as described in detail by Jonas<sup>48</sup> and by our group.<sup>26,36,49</sup> Solutions were supplied simultaneously to the two channels with a high-precision SP220IZ syringe pump (World Precision Instruments Inc., Sarasota, FL, US) and the open tip solution exchange time range 150–300 μs, depending on its size of the θ-glass capillary and the speed of flux.

Recordings of the single-channel activity were performed in the cell-attached configuration at a holding potential of 100 mV using an Axopatch 200B amplifier (Molecular Devices, Sunnyvale, CA, US), and the signal was filtered at 10 kHz with a built-in low-pass Bessel filter. Signals were digitized at the 100 kHz sampling rate by a Digidata 1550B acquisition card and Clampex 10.7 software (Molecular Devices, Sunnyvale, CA, US). Thick-wall borosilicate

glass pipettes (outer diameter = 1.5 mm; inner diameter = 0.87 mm; Hilgenberg, Malsfeld, Germany) were pulled using a P-1000 horizontal puller (Sutter Instruments, Novato, CA, US), and the pipet resistance was filled with the intrapipette Ringer's solution range 8–12 MΩ. For the reduction of noise, the pipettes were coated with Sylgard 184 (Dow Corning, Auburn, MI, US) and fire-polished on a microforge. External (and intrapipette) solution was different from the solution used for macroscopic recordings and contained (mM): 102.7 NaCl, 20 Na-gluconate, 2 KCl, 2 CaCl<sub>2</sub>, 1.2 MgCl<sub>2</sub>, 10 HEPES, 20 TEA-Cl, 14 mM D-(+)-glucose, and 15 sucrose (Carl Roth, Karlsruhe, Germany), dissolved in deionized water with the pH adjusted to 7.4 with NaOH. To achieve a further noise reduction, the amount of the external solution in the dish was kept at a minimal level (0.9–1 mL in dish of 35 mm diameter). Only the recordings of patches with seal resistance > 10 GΩ were considered for the analysis.

All of the chemicals were purchased from Merck (Darmstadt, Germany) unless stated otherwise.

**Data Analysis.** Macroscopic current traces were analyzed in terms of the amplitude measurements and the current kinetics. The protocol used to construct dose–response relationships for current amplitudes was chosen to avoid any distortion by the current rundown. Each recording started with acquisition of 2–3 sweeps of current responses to saturating [GABA] (10 mM); then a current elicited by a nonsaturating [GABA] was recorded and then, again, a response to saturating [GABA] was acquired. The relative response (nonsaturating/saturating) was calculated. Due to this time-consuming protocol, typically, up to two nonsaturating concentrations could be considered when recording from a single cell. Thus, a complete dose–response relationship was constructed from data collected from different cells. In the dose–response relationships presented in Figure 2, the data for each concentration were obtained from at least 3 cells. The outcome of our dose–response analysis for a specific receptor type is one set of parameters (EC<sub>50</sub> and n<sub>h</sub>) obtained from fitting the Hill equation (eq 1) to the dose–response relationship constructed from mean values of relative responses.

$$y = \frac{1}{1 + \left(\frac{EC_{50}}{[GABA]}\right)^{n_h}} \quad (1)$$

where  $y$  is the value of the relative current amplitude, EC<sub>50</sub> is the halfmaximal effective concentration, and  $n_h$  is the Hill coefficient. In the present report, comparison to the WT dose–response relationship was made based on the Hill's curve determined by our group in a recent study,<sup>30</sup> based on recordings on the WT receptors carried out in the same experimental conditions. The kinetic analysis was performed for current traces recorded in the majority in the excised-patch configuration that assured the best temporal resolution due to fastest solution exchange of the ultrafast perfusion. For the β<sub>2</sub>G254V mutant, excised-patch current recordings were difficult to obtain because of small amplitudes; therefore, recordings for this mutant were performed in the whole-cell configuration (lifted-cell mode) and were compared to a set of analogous control measurements for the WT receptors. A long (500 ms) agonist application protocol was used. The current onset was assessed as the 10–90% rise time (RT). Macroscopic desensitization was described using biexponential fitting, yielding two kinetic time constants (fast and slow, denoted τ<sub>fast</sub> and τ<sub>slow</sub>) with respective amplitudes, A<sub>fast</sub> and A<sub>slow</sub>, and a constant value  $C$  (representing the steady-state of current fading, which is a measure of nondesensitizing current) (eq 2)

$$I(t) = A_{fast}e^{-t/\tau_{fast}} + A_{slow}e^{-t/\tau_{slow}} + C \quad (2)$$

The percentage of each desensitization component was calculated by means of normalization: %A<sub>fast</sub> + %A<sub>slow</sub> + %C = 1. Additionally, to describe the macroscopic desensitization at distinct time points, we used FR10, FR300 and FR500 parameters which describe the fraction of a total amplitude remaining after 10, 300 and 500 ms, respectively. Deactivation kinetics, a phase of current relaxation after agonist removal, was described in terms of a mean time constant (τ<sub>mean</sub>),

calculated for either a single exponential fitting or a sum of two exponential components, following eq 3

$$I(t) = \sum_{n=1}^f A_n e^{-t/\tau_n} \quad (3)$$

Analogous to eq 2,  $A_n$  is the amplitude of the  $n$ -th component, and  $\tau_n$  is the respective time constant. When deactivation was fitted with two exponentials, the mean deactivation time constant was calculated as  $\tau_{\text{deact}} = A_1\% \tau_1 + A_2\% \tau_2$ , where  $A_n\%$  is the percentage of the respective component ( $A_1\% + A_2\% = 1$ ).

Single-channel data analysis was started with the predominant mode selection. Typically, traces exhibited 1–3 modes of activity.<sup>22,23,50</sup> Event detection analysis in Clampfit 10.7 software (Molecular Devices, Sunnyvale, CA, US) was used to assess open probability ( $P_{\text{open}}$ ) for distinct clusters, three modes for  $\beta_2\text{G254V} = 0.66 \pm 0.08$ , 61% (predominant);  $0.90 \pm 0.05$ , 26%; and  $0.16 \pm 0.12$ , 13%; and 3 modes for  $\beta_2\text{L296V} = 0.20 \pm 0.05$ , 60% (predominant);  $0.41 \pm 0.04$ , 19%; and  $0.05 \pm 0.01$ , 21%. For  $\alpha_1\text{G258V}$  and  $\alpha_1\text{L300V}$ , only one mode of activity was present,  $P_{\text{open}}$  for  $\alpha_1\text{G258V} = 0.33 \pm 0.08$  and for  $\alpha_1\text{L300V} = 0.19 \pm 0.01$ . The predominant mode for WT activity was identified according to the description by Lema and Auerbach<sup>50</sup> and Kisiel et al.<sup>23</sup> and had the  $P_{\text{open}}$  value of  $0.69 \pm 0.04$ . Selected clusters of predominant mode activity were filtered to reach a signal-to-noise ratio of at least 15. The final cutoff frequency ( $f_c$ ) was calculated as follows:

$$1/f_c = 1/f_a + 1/f_d \quad (4)$$

where  $f_a$  is the analogue filter frequency (typically 10 kHz) and  $f_d$  is the digital frequency (offline filtering with 8-pole low-pass Bessel filter by pClamp software). The sampling frequency,  $f_s$ , was reduced to  $f_s = 10 \times f_c$ . Recordings with multilevel openings were excluded from the analysis. The clusters were idealized by a time-course fitting procedure using SCAN software from the DCprogs software pack that was kindly provided to our group by Dr. David Colquhoun. Processed data was used to generate distributions of apparent shut and open times using EKDIST software (DCprogs) for 8000–10 000 events obtained from the idealization. Distributions were fitted with a sum of exponential components (in figures, %P = percentage,  $\tau$  = time constant) which, for the  $\beta_2\text{G254V}$  mutant and WT, was typically four exponentials of shut times and two of open times. The shut time distributions for  $\alpha_1\text{G258V}$ ,  $\alpha_1\text{L300V}$ , and  $\beta_2\text{L296V}$  mutants exhibited three exponential components, two predominant and the third (the fastest one) with a markedly lower percentage.

Bursts analysis was performed by considering the critical time ( $t_{\text{crit}}$ ) calculated from the shut times distribution analysis using EKDIST, according to the Clapham & Neher criterion<sup>51</sup> applied to the third and fourth shut time components for  $\beta_2\text{G254V}$  and WT and to the second and third shut time components for  $\alpha_1\text{G258V}$ ,  $\alpha_1\text{L300V}$  and  $\beta_2\text{L296V}$ . This analysis provided information about the open probability for clusters ( $P_{\text{open}}$ ) and the burst length.

**Macroscopic Data Modeling.** Kinetic modeling of macroscopic current responses was based on the frame of the WT flipped Jones-Westbrook Model proposed by Szczot et al.<sup>26</sup> In the first step, multiple models were created using in-house Python scripts in order to find changes in rate constant essential for depiction of observed changes in currents kinetics of respective mutants relative to WT. Afterward, once the results from the previous step were used as initial guesses, the optimization of the model rates for each current recording (average of all sweeps from single cell) was performed using “waveform fitting” module of ChannelLab software. Because the dose–response relationships for mutants only slightly differed from that for the WT receptors (Figure 2), suggesting little effect on the binding step, the rates  $k_{\text{on}}$  and  $k_{\text{off}}$  were fixed at the WT values<sup>26</sup> for WT and all of the mutants. In the case of WT,  $\alpha_1\text{G258V}$  and  $\beta_2\text{L296V}$ , the fit was done in an  $\sim 30$  ms window (see model simulations for details). The same window was applied for  $\beta_2\text{G254V}$  mutant, but because these currents were recorded in the whole-cell configuration, a separate modeling was done for currents mediated by the WT receptors and measured in these experimental conditions.

Because in the responses mediated by  $\alpha_1\text{L300V}$  only the slow macroscopic desensitization component was affected, fitting was done in an  $\sim 1000$  ms window for the model with two desensitized states, and for comparison, the same analysis was carried out for the WT receptors (see model simulations for details).

**Single-Channel Data Modeling.** For kinetic modeling of single-channel activity of WT and the  $\beta_2\text{G254V}$  mutant, a framework of kinetic model (two open and two desensitized states) from Kisiel et al.<sup>23</sup> was adapted. Modeling was performed using HJCFIT software (DCprogs), which is based on the maximum likelihood method that enabled optimization of the rate constants, with the time resolution of 40–90  $\mu\text{s}$ . Kinetic modeling for the  $\alpha_1\text{G258V}$ ,  $\alpha_1\text{L300V}$  and  $\beta_2\text{L296V}$  mutants, due to the reduced number of components in shut time distributions, was based on the kinetic scheme from Kisiel et al.<sup>23</sup> that was reduced to only one desensitization state. The models for WT and all of the mutants were validated by model simulations at both experimental and 0  $\mu\text{s}$  resolutions and were considered satisfactory when simulated distributions reproduced well the parameters of distributions obtained from the experimental data.

**Structure Visualizations.** In each structural visualization, the structure of human GABA<sub>A</sub>R  $\alpha_1\beta_2\gamma_2$  subtype in complex with GABA (pdb code 6X3Z)<sup>14</sup> was used. All of the molecular graphics were prepared in VMD.<sup>52</sup>

**Statistical Analysis.** The statistical analysis and data presentation was performed using SigmaPlot 11.0 software (Systat Software). The data were analyzed with Grubb’s test for outlier identification. The single comparisons of a parameter for one mutant vs WT were based on the Student’s  $t$  test or, alternatively, the Mann–Whitney U test for the data that failed the normality or equal variance test. Values of  $p < 0.05$  were considered statistically significant.

Data are presented as mean values and  $\pm$ SEM in bars and scatter plots.

## AUTHOR INFORMATION

### Corresponding Authors

**Katarzyna Terejko** – Department of Biophysics and Neuroscience, Wrocław Medical University, 50-368 Wrocław, Poland; [orcid.org/0000-0003-0805-4444](https://orcid.org/0000-0003-0805-4444); Phone: +48 71 784 15 79; Email: [katarzyna.terejko@student.umed.wroc.pl](mailto:katarzyna.terejko@student.umed.wroc.pl)

**Jerzy W. Mozrzymas** – Department of Biophysics and Neuroscience, Wrocław Medical University, 50-368 Wrocław, Poland; Department of Molecular Physiology and Neurobiology, University of Wrocław, 50-335 Wrocław, Poland; Phone: + 48 71 784 15 50; Email: [jerzy.mozrzymas@umed.wroc.pl](mailto:jerzy.mozrzymas@umed.wroc.pl)

### Authors

**Michał A. Michałowski** – Department of Biophysics and Neuroscience, Wrocław Medical University, 50-368 Wrocław, Poland; Department of Molecular Physiology and Neurobiology, University of Wrocław, 50-335 Wrocław, Poland

**Ilona Izykowska** – Department of Biophysics and Neuroscience, Wrocław Medical University, 50-368 Wrocław, Poland

**Anna Dominik** – Department of Biophysics and Neuroscience, Wrocław Medical University, 50-368 Wrocław, Poland

**Aleksandra Brzostowicz** – Department of Biophysics and Neuroscience, Wrocław Medical University, 50-368 Wrocław, Poland

Complete contact information is available at: <https://pubs.acs.org/10.1021/acchemneuro.1c00151>

### Author Contributions

<sup>§</sup>K.T. and M.A.M. contributed equally.

## Author Contributions

K.T. performed part of the single-channel experiments, data analysis, kinetic modeling of single-channel activity and data presentation and contributed to the writing and editing of the manuscript. M.A.M. performed kinetic modeling of macroscopic currents, structure visualization and data presentation and contributed to the writing of the manuscript. I.I. prepared all of the plasmids and performed part of the experiments and data analysis. A.D. performed part of the experiments. A.B. performed part of the experiments. J.W.M. conceived and supervised the project, procured financial support, participated in designing the experiments, data analysis, and model simulations and wrote and edited the final version of the manuscript.

## Funding

This work was supported by Polish National Science Centre grant MAESTRO DEC-2015/18/A/NZ1/00395.

## Notes

The authors declare no competing financial interest.

## ACKNOWLEDGMENTS

We thank Dr Przemysław T. Kaczor from Department of Biophysics and Neuroscience, Wrocław Medical University, for his assistance in the single-channel analysis of the WT receptors.

## ABBREVIATIONS

ECD, extracellular domain; EGFP, enhanced green fluorescence protein; FR10/300/500, fraction of current trace remaining after 10 300 or 500 ms relative to a full current amplitude; LBS, ligand binding site; GABA<sub>A</sub>R,  $\gamma$ -aminobutyric acid type A receptor; [GABA], concentration of GABA agonist; M1-M3, transmembrane helices of GABA<sub>A</sub>R; pCMV, adenoviral vector with the promoter for cytomegalovirus; pLGIC, pentameric ligand gated ion channel; TMD, transmembrane domain; WT, wild type of the  $\alpha_1\beta_2\gamma_2$  GABA<sub>A</sub>

## REFERENCES

- (1) Cederholm, J. M. E., Schofield, P. R., and Lewis, T. M. (2009) Gating Mechanisms in Cys-Loop Receptors. *Eur. Biophys. J.* 39 (1), 37–49.
- (2) Miller, P. S., and Smart, T. G. (2010) Binding, Activation and Modulation of Cys-Loop Receptors. *Trends Pharmacol. Sci.* 31 (4), 161–174.
- (3) Thompson, A. J., Lester, H. A., and Lummis, S. C. R. (2010) The structural basis of function in Cys-loop receptors. *Q. Rev. Biophys.* 43, 449.
- (4) Bianchi, M. T., Song, L., Zhang, H., and Macdonald, R. L. (2002) Two Different Mechanisms of Disinhibition Produced by GABA<sub>A</sub> Receptor Mutations Linked to Epilepsy in Humans. *J. Neurosci.* 22 (13), 5321–5327.
- (5) Bozzi, Y., Provenzano, G., and Casarosa, S. (2018) Neurobiological Bases of Autism-Epilepsy Comorbidity: A Focus on Excitation/Inhibition Imbalance. *Eur. J. Neurosci.* 47 (6), 534–548.
- (6) Möhler, H. (2015) The Legacy of the Benzodiazepine Receptor: From Flumazenil to Enhancing Cognition in down Syndrome and Social Interaction in Autism. *Adv. Pharmacol.* 72, 1–36.
- (7) Luscher, B., Shen, Q., and Sahir, N. (2011) The GABAergic Deficit Hypothesis of Major Depressive Disorder. *Mol. Psychiatry* 16 (4), 383–406.
- (8) Schmidt, M. J., and Mirnics, K. (2015) Neurodevelopment, GABA System Dysfunction, and Schizophrenia. *Neuropsychopharmacology* 40 (1), 190–206.

- (9) Hosie, A. M., Wilkins, M. E., Da Silva, H. M. A., and Smart, T. G. (2006) Endogenous Neurosteroids Regulate GABA<sub>A</sub> Receptors through Two Discrete Transmembrane Sites. *Nature* 444 (7118), 486–489.
- (10) Belelli, D., and Lambert, J. J. (2005) Neurosteroids: Endogenous Regulators of the GABA<sub>A</sub> Receptor. *Nat. Rev. Neurosci.* 6 (7), 565–575.
- (11) Sieghart, W., and Savić, M. M. (2018) International Union of Basic and Clinical Pharmacology. CVI: GABA A Receptor Subtype and Function-Selective Ligands: Key Issues in Translation to Humans. *Pharmacol. Rev.* 70 (4), 836–878.
- (12) Garcia, P., Kolesky, S., and Jenkins, A. (2010) General Anesthetic Actions on GABA<sub>A</sub> Receptors. *Curr. Neuropharmacol.* 8 (1), 2–9.
- (13) Zeller, A., Arras, M., Jurd, R., and Rudolph, U. (2007) Identification of a Molecular Target Mediating the General Anesthetic Actions of Pentobarbital. *Mol. Pharmacol.* 71 (3), 852–859.
- (14) Kim, J. J., Gharpure, A., Teng, J., Zhuang, Y., Howard, R. J., Zhu, S., Noviello, C. M., Walsh, R. M., Lindahl, E., and Hibbs, R. E. (2020) Shared Structural Mechanisms of General Anaesthetics and Benzodiazepines. *Nature* 585 (7824), 303–308.
- (15) Laverty, D., Desai, R., Uchański, T., Masiulis, S., Stec, W. J., Malinauskas, T., Zivanov, J., Pardon, E., Steyaert, J., Miller, K. W., and Aricescu, A. R. (2019) Cryo-EM Structure of the Human  $\alpha_1\beta_3\gamma_2$  GABA<sub>A</sub> Receptor in a Lipid Bilayer. *Nature* 565, 1.
- (16) Miller, P. S., Masiulis, S., Malinauskas, T., and Kotecha, A. (2018) Heteromeric GABA A Receptor Structures in Positively-Modulated Active States. *bioRxiv*, 1 DOI: 10.1101/338343.
- (17) Zhu, S., Noviello, C. M., Teng, J., Walsh, R. M., Kim, J. J., and Hibbs, R. E. (2018) Structure of a Human Synaptic GABA<sub>A</sub> Receptor. *Nature* 559, 1.
- (18) Unwin, N. (2005) Refined Structure of the Nicotinic Acetylcholine Receptor at 4Å Resolution. *J. Mol. Biol.* 346 (4), 967–989.
- (19) Steinbach, J. H., and Akk, G. (2001) Modulation of GABA<sub>A</sub> Receptor Channel Gating by Pentobarbital. *J. Physiol.* 537 (3), 715–733.
- (20) Haas, K. F., and Macdonald, R. L. (1999) GABA(A) Receptor Subunit  $\gamma_2$  and  $\delta$  Subtypes Confer Unique Kinetic Properties on Recombinant GABA(A) Receptor Currents in Mouse Fibroblasts. *J. Physiol.* 514 (1), 27–45.
- (21) Terejko, K., Michałowski, M. A., Dominik, A., Andrzejczak, A., and Mozrzymas, J. W. (2021) Interaction between GABA<sub>A</sub> Receptor  $\alpha_1$  and  $\beta_2$  Subunits at the N-Terminal Peripheral Regions Is Crucial for Receptor Binding and Gating. *Biochem. Pharmacol.* 183 (November 2020), 114338.
- (22) Brodzki, M., Michałowski, M. A., Gos, M., and Mozrzymas, J. W. (2020) Mutations of  $\alpha_1F45$  Residue of GABA<sub>A</sub> Receptor Loop G Reveal Its Involvement in Agonist Binding and Channel Opening/Closing Transitions. *Biochem. Pharmacol.* 177, 177.
- (23) Kisiel, M., Jatczak, M., Brodzki, M., and Mozrzymas, J. W. (2018) Spontaneous Activity, Singly Bound States and the Impact of Alpha1Phe64 Mutation on GABA<sub>A</sub> Receptor Gating in the Novel Kinetic Model Based on the Single-Channel Recordings. *Neuropharmacology* 131, 453–474.
- (24) Terejko, K., Kaczor, P. T., Michałowski, M. A., Dąbrowska, A., and Mozrzymas, J. W. (2020) The C Loop at the Orthosteric Binding Site Is Critically Involved in GABA<sub>A</sub> Receptor Gating. *Neuropharmacology* 166, 166.
- (25) Jatczak-Śliwa, M., Kisiel, M., Czyżewska, M. M., Brodzki, M., and Mozrzymas, J. W. (2020) GABA<sub>A</sub> Receptor  $\beta_2E155$  Residue Located at the Agonist-Binding Site Is Involved in the Receptor Gating. *Front. Cell. Neurosci.* 14 (February), 1–18.
- (26) Szczot, M., Kisiel, M., Czyżewska, M. M., and Mozrzymas, J. W. (2014)  $\alpha_1F64$  Residue at GABA(A) Receptor Binding Site Is Involved in Gating by Influencing the Receptor Flipping Transitions. *J. Neurosci.* 34 (9), 3193–3209.

- (27) Gielen, M., Thomas, P., and Smart, T. G. (2015) The Desensitization Gate of Inhibitory Cys-Loop Receptors. *Nat. Commun.* 6, 6.
- (28) Jatzczak-Śliwa, M., Terejko, K., Brodzki, M., Michałowski, M. A., Czyżewska, M. M., Nowicka, J. M., Andrzejczak, A., Srinivasan, R., and Mozrzymas, J. W. (2018) Distinct Modulation of Spontaneous and GABA-Evoked Gating by Flurazepam Shapes Cross-Talk between Agonist-Free and Liganded Gaba<sub>A</sub> Receptor Activity. *Front. Cell. Neurosci.* 12 (August), 1–18.
- (29) Germann, A. L., Pierce, S. R., Senneff, T. C., Burbridge, A. B., Steinbach, J. H., and Akk, G. (2019) Steady-State Activation and Modulation of the Synaptic-Type  $\alpha 1\beta 2\gamma 2L$  GABA<sub>A</sub> Receptor by Combinations of Physiological and Clinical Ligands. *Physiol. Rep.* 7 (18), 1–13.
- (30) Brodzki, M., Rutkowski, R., Jatzczak, M., Kisiel, M., Czyżewska, M. M., and Mozrzymas, J. W. (2016) Comparison of Kinetic and Pharmacological Profiles of Recombinant  $\alpha 1\gamma 2L$  and  $\alpha 1\beta 2\gamma 2L$  GABA<sub>A</sub> Receptors—A Clue to the Role of Intersubunit Interactions. *Eur. J. Pharmacol.* 784, 81–89.
- (31) Colquhoun, D., and Lape, R. (2012) Allosteric Coupling in Ligand-Gated Ion Channels. *J. Gen. Physiol.* 140 (6), 599–612.
- (32) Colquhoun, D., and Sakmann, B. (1985) Fast events in single-channel currents activated by acetylcholine and its analogues at the frog muscle end-plate. *J. Physiol. Dec*;369, 501–57.
- (33) Mozrzymas, J. W., Barberis, A., Mercik, K., and Żarnowska, E. D. (2003) Binding Sites, Singly Bound States, and Conformation Coupling Shape GABA-Evoked Currents. *J. Neurophysiol.* 89 (2), 871–883.
- (34) Colquhoun, D., and Hawkes, A. G. (1982) On the Stochastic Properties of Bursts of Single Ion Channel Openings and of Clusters of Bursts. *Philos. Trans. R. Soc. Lond. B. Biol. Sci.* 300 (1098), 1–59.
- (35) Colquhoun, D., and Hawkes, A. G. (1995) Desensitization of N-Methyl-D-Aspartate Receptors: A Problem of Interpretation. *Proc. Natl. Acad. Sci. U. S. A.* 92 (22), 10327–10329.
- (36) Colquhoun, D. (1998) Binding, Gating, Affinity and Efficacy: The Interpretation of Structure-Activity Relationships for Agonists and of the Effects of Mutating Receptors. *Br. J. Pharmacol.* 125 (Scheme 1), 923–947.
- (37) Bianchi, M. T., Botzolkakis, E. J., Haas, K. F., Fisher, J. L., and Macdonald, R. L. (2007) Microscopic Kinetic Determinants of Macroscopic Currents: Insights from Coupling and Uncoupling of GABA<sub>A</sub> Receptor Desensitization and Deactivation. *J. Physiol.* 584 (Pt 3), 769–787.
- (38) Kisiel, M., Jatzczak-Śliwa, M., and Mozrzymas, J. W. (2019) Protons Modulate Gating of Recombinant  $\alpha 1\beta 2\gamma 2$  GABA<sub>A</sub> Receptor by Affecting Desensitization and Opening Transitions. *Neuropharmacology* 146 (October 2018), 300–315.
- (39) Bianchi, M. T., and Macdonald, R. L. (2002) Slow Phases of GABA<sub>A</sub> Receptor Desensitization: Structural Determinants and Possible Relevance for Synaptic Function. *J. Physiol.* 544 (1), 3–18.
- (40) Masiulis, S., Desai, R., Uchański, T., Serna Martin, I., Laverty, D., Karia, D., Malinauskas, T., Zivanov, J., Pardon, E., Kotecha, A., Steyaert, J., Miller, K. W., and Aricescu, A. R. (2019) GABA<sub>A</sub> Receptor Signalling Mechanisms Revealed by Structural Pharmacology. *Nature* 565, 454.
- (41) Newell, J. G., McDevitt, R. A., and Czajkowski, C. (2004) Mutation of Glutamate 155 of the GABA<sub>A</sub> Receptor B2 Subunit Produces a Spontaneously Open Channel: A Trigger for Channel Activation. *J. Neurosci.* 24 (50), 11226–11235.
- (42) Torres, V. I., and Weiss, D. S. (2002) Identification of a Tyrosine in the Agonist Binding Site of the Homomeric P1  $\gamma$ -Aminobutyric Acid (GABA) Receptor That, When Mutated, Produces Spontaneous Opening. *J. Biol. Chem.* 277 (46), 43741–43748.
- (43) Gielen, M., and Corringer, P. J. (2018) The Dual-Gate Model for Pentameric Ligand-Gated Ion Channels Activation and Desensitization. *J. Physiol.* 596 (10), 1873–1902.
- (44) Noviello, C. M., Gharpure, A., Mukhtasimova, N., Cabuco, R., Baxter, L., Borek, D., Sine, S. M., and Hibbs, R. E. (2021) Structure and Gating Mechanism of the  $\alpha 7$  Nicotinic Acetylcholine Receptor. *Cell* 184 (8), 2121–2134 e13..
- (45) Sauguet, L., Shahsavari, A., Poitevin, F., Huon, C., Menny, A., Nemečz, A., Haouz, A., Changeux, J. P., Corringer, P. J., and Delarue, M. (2014) Crystal Structures of a Pentameric Ligand-Gated Ion Channel Provide a Mechanism for Activation. *Proc. Natl. Acad. Sci. U. S. A.* 111 (3), 966–971.
- (46) Nemečz, A., Prevost, M. S., Menny, A., and Corringer, P. J. (2016) Emerging Molecular Mechanisms of Signal Transduction in Pentameric Ligand-Gated Ion Channels. *Neuron* 90 (3), 452–470.
- (47) Taly, A., Delarue, M., Grutter, T., Nilges, M., Le Novère, N., Corringer, P. J., and Changeux, J. P. (2005) Normal Mode Analysis Suggests a Quaternary Twist Model for the Nicotinic Receptor Gating Mechanism. *Biophys. J.* 88 (6), 3954–3965.
- (48) Jonas, P., Sakmann, B., and Neher, E. (1995) Fast Application of Agonists to Isolated Membrane Patches. *Single-Channel Recording*, 231–243, DOI: 10.1007/978-1-4419-1229-9\_10.
- (49) Mozrzymas, J. W., Wójtowicz, T., Piast, M., Lebida, K., Wyrembek, P., and Mercik, K. (2007) GABA Transient Sets the Susceptibility of MIPSCs to Modulation by Benzodiazepine Receptor Agonists in Rat Hippocampal Neurons. *J. Physiol.* 585 (1), 29–46.
- (50) Lema, G. M. C., and Auerbach, A. (2006) Modes and Models of GABA<sub>A</sub> Receptor Gating. *J. Physiol.* 572 (1), 183–200.
- (51) Clapham, D. E., and Neher, E. (1984) Substance P Reduces Acetylcholine-induced Currents in Isolated Bovine Chromaffin Cells. *J. Physiol.* 347 (1), 255–277.
- (52) Humphrey, W., Dalke, A., and Schulten, K. (1996) VMD: Visual Molecular Dynamics. *J. Mol. Graphics* 14 (1), 33–38.